

Screening for functional circular RNAs using the CRISPR-Cas13 system

Siqi Li^{1,6}, Xiang Li^{1,6}, Wei Xue^{2,6}, Lin Zhang^{3,6}, Liang-Zhong Yang¹, Shi-Meng Cao¹, Yun-Ni Lei^{2,4}, Chu-Xiao Liu¹, Si-Kun Guo¹, Lin Shan¹, Man Wu¹, Xiao Tao¹, Jia-Lin Zhang^{1,5}, Xiang Gao^{1,4}, Jun Zhang¹, Jia Wei², Jinsong Li^{1,3,4,5}✉, Li Yang^{1,2,4}✉ and Ling-Ling Chen^{1,4,5}✉

Circular RNAs (circRNAs) produced from back-spliced exons are widely expressed, but individual circRNA functions remain poorly understood owing to the lack of adequate methods for distinguishing circRNAs from cognate messenger RNAs with overlapping exons. Here, we report that CRISPR-RfxCas13d can effectively discriminate circRNAs from mRNAs by using guide RNAs targeting sequences spanning back-splicing junction (BSJ) sites featured in RNA circles. Using a lentiviral library that targets sequences across BSJ sites of highly expressed human circRNAs, we show that a group of circRNAs are important for cell growth mostly in a cell-type-specific manner and that a common oncogenic circRNA, circFAM120A, promotes cell proliferation by preventing the mRNA for family with sequence similarity 120A (FAM120A) from binding the translation inhibitor IGF2BP2. Further application of RfxCas13d-BSJ-gRNA screening has uncovered circMan1a2, which has regulatory potential in mouse embryo preimplantation development. Together, these results establish CRISPR-RfxCas13d as a useful tool for the discovery and functional study of circRNAs at both individual and large-scale levels.

Back-splicing of pre-mRNA exons leads to genome-wide expression of circRNAs that are identical to linear mRNA sequences except at BSJ sites. The functions of circRNAs largely remain elusive, partly owing to the lack of effective tools to interfere with circular, but not linear, RNAs in cells¹. Short hairpin RNAs (shRNAs) or specific small interfering RNAs (siRNAs) targeting BSJ sites of circRNAs have been used to knock down circRNAs^{2–4}. However, even partial complementarity of half an interfering RNA (RNAi) (~10 nucleotides) to linear mRNAs may affect parental-gene expression (Extended Data Fig. 1a). Genome engineering has been used to deplete a circRNA by removing either the entire circRNA-forming exon⁵ or the intronic *cis*-elements required for circRNA biogenesis^{6,7} (Extended Data Fig. 1b), but only a few circRNAs have been studied with these approaches. A simple and scalable tool that can be used to identify functional circRNAs is still lacking.

Recent studies have established that RNA-targeting type VI CRISPR effectors, known as Cas13a, Cas13b and Cas13d RNases^{8–11}, can be directed to cleave single-stranded (ss) RNA targets carrying complementary spacers in mammalian cells^{11–13}. Type VI CRISPR-Cas complex requires a 22- to 30-nucleotide spacer in guide RNA (gRNA) that is complementary to the target, and is intolerant to mismatches in the central seed^{11–13}, which exhibits higher specificity than does RNAi. However, it remains unknown whether the CRISPR-Cas13 system can discriminate circRNAs from their linear cognates with gRNAs targeting sequences spanning the BSJ, and if so, the robustness of this approach on circRNA levels.

Results

RfxCas13d-BSJ-gRNA discriminates circRNAs from mRNAs. We first sought to identify the best effector for circRNA knockdown by screening Cas13 family proteins^{11,12,14}. We synthesized the mammalian codon-optimized DNA sequences for each of the proteins (LwaCas13a, PspCas13b, PguCas13b, RanCas13b, EsCas13d, AdmCas13d and RfxCas13d) and cloned them individually into an expression vector with a sequence for carboxy-terminal monomeric superfolder green fluorescent protein (msfGFP) to enhance protein stability (Extended Data Fig. 1c). We confirmed that each Cas13 was expressed in 293FT cells (Extended Data Fig. 1d,e), and various knockdown efficiencies of KRAS mRNA were observed when Cas13 and matched gRNAs were cotransfected into cells (Extended Data Fig. 1f).

Next, we examined the knockdown efficiency and specificity of each Cas13 on two circRNAs, *circPOLR2A* (336 nucleotides), derived from RNA polymerase II subunit A (*POLR2A*), and *circRTN4* (2,457 nucleotides), derived from reticulon 4 (*RTN4*), in 293FT cells. We designed three 30-nucleotide gRNAs spanning BSJ (BSJ-gRNAs) for each circRNA (Fig. 1a). Most Cas13s attenuated expression of both circRNAs but had no detectable effect on their cognate mRNAs, and RfxCas13d exhibited the highest knockdown efficiency (>80%) (Fig. 1b and Extended Data Fig. 1g). Northern blot further confirmed the notable knockdown of *circPOLR2A* by RfxCas13d-BSJ-gRNAs (Extended Data Fig. 1h). Importantly, a non-targeting (NT) gRNA did not direct Cas13 to circRNAs for cleavage (Fig. 1b and Extended Data Fig. 1g); overexpression of

¹State Key Laboratory of Molecular Biology, Shanghai Key Laboratory of Molecular Andrology, CAS Center for Excellence in Molecular Cell Science, Shanghai Institute of Biochemistry and Cell Biology, University of Chinese Academy of Sciences, Chinese Academy of Sciences, Shanghai, China.

²CAS Key Laboratory of Computational Biology, CAS-MPG Partner Institute for Computational Biology, Shanghai Institute of Nutrition and Health, Shanghai Institutes for Biological Sciences, University of Chinese Academy of Sciences, Chinese Academy of Sciences, Shanghai, China. ³State Key Laboratory of Cell Biology, Shanghai Key Laboratory of Molecular Andrology, CAS Center for Excellence in Molecular Cell Science, Shanghai Institute of Biochemistry and Cell Biology, University of Chinese Academy of Sciences, Chinese Academy of Sciences, Shanghai, China. ⁴School of Life Science and Technology, ShanghaiTech University, Shanghai, China. ⁵School of Life Science, Hangzhou Institute for Advanced Study, University of Chinese Academy of Sciences, Hangzhou, China. ⁶These authors contributed equally: Siqi Li, Xiang Li, Wei Xue, Lin Zhang. ✉e-mail: jqli@sibcb.ac.cn; liyang@picb.ac.cn; linglingchen@sibcb.ac.cn

RfxCas13d or BSJ-gRNAs alone did not affect circRNA expression (Extended Data Fig. 1i,j). To rule out off-target effects of BSJ-gRNAs, we designed additional control gRNAs that had half-sequences that were replaced by scrambled sequences (paired control) (Fig. 1c) or sequences from adjacent linear exons (gRNA-L) (Extended Data Fig. 1k) of *circPOLR2A* or *circRTN4*. None of these control gRNAs could direct RfxCas13d to degrade circRNAs (Fig. 1c and Extended Data Fig. 1k). As expected, control gRNAs (gRNA-L) targeting linear RNA exon–exon junctions led to decreased linear mRNA expression by RfxCas13d (Extended Data Fig. 1k). In addition, replacing a 10-nucleotide (scrambled/mismatch) on either side of an originally highly effective gRNA targeting KRAS and *B4GALNT1* completely blocked knockdown effects (Extended Data Fig. 1l).

To explore the general applicability of RfxCas13d–BSJ-gRNAs for circRNA interference, we examined knockdown efficiencies of another eight circRNAs in 293FT cells (Fig. 1d). Similar to *circPOLR2A* and *circRTN4*, expression of all examined circRNAs, but not paired linear mRNAs, was decreased more than 50% by RfxCas13d–BSJ-gRNAs (Fig. 1d). Similarly, RfxCas13d was also the most efficient Cas13 to specifically disrupt expression of circRNAs (Extended Data Fig. 2a–c) in HeLa cells.

siRNAs^{4,15,16} and shRNAs²³ have been used in loss-of-function (LOF) studies of circRNAs. We compared specificity and knockdown efficiency of the RfxCas13d system and shRNAs in a position-matched manner for nine pairs of circular and linear cognate RNAs (Fig. 1e). Compared with shRNA-mediated knockdown, RfxCas13d–BSJ-gRNA showed higher efficiency of circRNA knockdown (RfxCas13d, mean ~65%; shRNA, mean ~35%) and lower off-target rates on linear mRNAs for all examined pairs (Fig. 1e). Collectively, these results reveal that RfxCas13d is an effective tool for circRNA knockdown with high efficiency, specificity and generality.

Characteristics of RfxCas13d–BSJ-gRNA-mediated circRNA knockdown. We first determined the minimal spacer length requirement for an efficient RfxCas13d targeting circRNAs. We generated a series of BSJ-gRNAs with spacers that ranged from 16 to 36 nucleotides and spanned the BSJ of *circPOLR2A* (Fig. 1f, top). Consistent with the previous in vitro cleavage assay of EsCas13d¹¹, a minimal spacer of 18 nucleotides was required for RfxCas13d to target *circPOLR2A*, but the highest knockdown efficiency was observed with spacers of 22 nucleotides or longer (Fig. 1f). In all examined conditions, the expression of linear *POLR2A* mRNA was barely affected (Fig. 1f), suggesting that recognizing the unique BSJ in circRNAs (considered as a mismatch ribonucleotide for the paired linear mRNA) in the spacer effectively constrained RfxCas13d targeting to only circRNAs.

This notion was further confirmed by characterizing the mismatch tolerance of RfxCas13d for circRNA targeting. We introduced either single or double mismatches into BSJ-gRNAs and observed that most single or double mismatches impaired the knockdown efficiency of *circPOLR2A* by RfxCas13d, whereas single and double mismatches in the gRNAs 3' end (19–22 nucleotides) only mod-

estly affected *circPOLR2A* expression (Extended Data Fig. 2d). A central seed region of the BSJ-gRNA spacer was identified as being more sensitive to mismatches, extending from the position of -8 to 8 nucleotides in a 22-nucleotide-long BSJ-gRNA spacer (Extended Data Fig. 2d). As expected, expression of linear *POLR2A* mRNA remained unaltered under all conditions (Extended Data Fig. 2d).

We evaluated the knockdown efficiency and specificity of RfxCas13d for circRNA and its paired mRNA by designing gRNAs tiled in 10-nucleotide increments across the BSJ of *circPOLR2A* (Fig. 1g) or *circPVT1* (Extended Data Fig. 2e). Only BSJ-gRNAs could guide RfxCas13d to deplete circRNAs without affecting linear RNAs, whereas other gRNAs that did not contain BSJ complementary sequences could direct RfxCas13d to degrade both circular and linear RNAs due to totally overlapping sequences.

We examined the position-effect of the BSJ-gRNA spacer for RfxCas13d-mediated circRNA knockdown by tiling gRNAs across the BSJ of *circPOLR2A*. gRNA spacers with the BSJ in the center (-7 to 7 nucleotides spanning the BSJ site) exhibited high knockdown efficiencies without affecting linear cognate RNAs (Fig. 1g). Similar results were observed for *circHIPK3* (derived from homeodomain-interacting protein kinase 3, HIPK3) and *circRTN4* by tiling assays (Extended Data Fig. 2f,g). The advantage of using RfxCas13d in mediating circular, but not linear, RNA interference could be due to distinct biogenesis efficiencies, conformations and turnover rates between circular and linear RNAs^{6,17}.

RfxCas13d–BSJ-gRNA screens identify circRNAs that act in a cell-type-specific manner in cell proliferation. Next, we explored the feasibility of using the RfxCas13d–BSJ-gRNA system for large-scale LOF screens of circRNAs. We constructed a library of BSJ-gRNAs that target highly expressed circRNAs in human cells (Fig. 2a). Among the top 10% of highly expressed circRNAs with more than 3 copies in 1 HT29, HeLa, 293FT or H9 cell, determined using CIRCexplorer2 (ref. ¹⁸) (Extended Data Fig. 3a,b), 762 circRNAs were successfully included in the gRNA library (Fig. 2a and Supplementary Table 1). This pool of circRNAs contains the most highly expressed circRNAs in examined human cell lines (Extended Data Fig. 3c) and has a representative length distribution compared with all expressed circRNAs (Extended Data Fig. 3d).

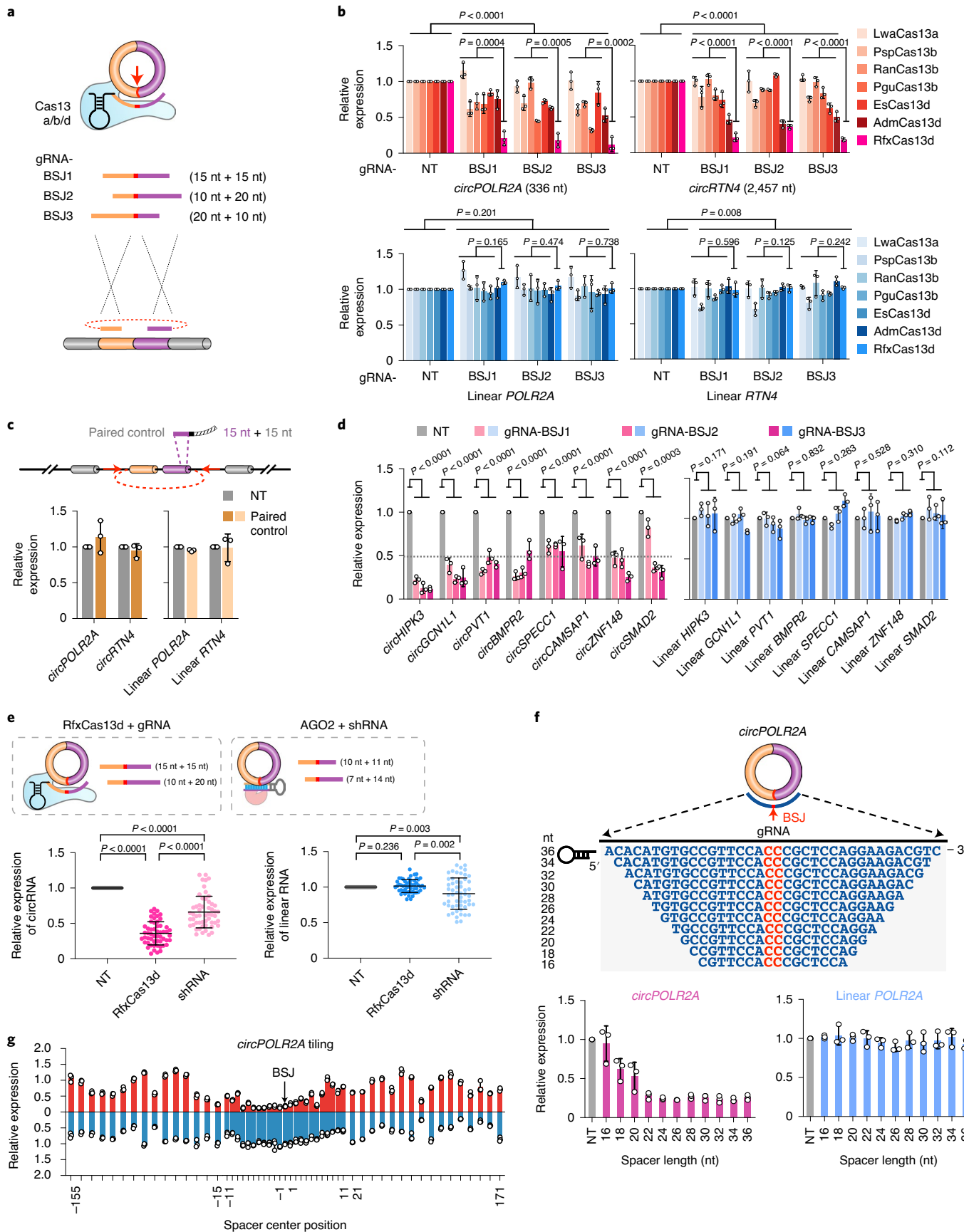
To construct the library, we designed 5 BSJ-gRNAs of 26–30 nucleotides that target sequences spanning the BSJ in each circRNA (Fig. 2a and Supplementary Table 1). Such BSJ-gRNAs have been demonstrated to knock down *circPOLR2A*, *circHIPK3*, *circRTN4* and other examined circRNAs without affecting linear cognate RNAs. For each circRNA, one paired control gRNA was designed (Fig. 2a). The gRNA library was constructed from synthetic oligonucleotide pools by Gibson assembly. Deep sequencing of enriched gRNAs amplified from the library showed a high representation and uniformity of gRNAs (Extended Data Fig. 3e).

We conducted screens to identify circRNAs that are required for cell proliferation. HT29, HeLa and 293FT cells stably expressing RfxCas13d (Extended Data Fig. 3f) were infected with the gRNA lentiviral library at a multiplicity of infection of 0.3. These cells

Fig. 1 | RfxCas13d–BSJ-gRNA discriminates circRNAs from mRNAs. **a**, Schematic of circRNA knockdown (KD) by Cas13 orthologs. Three BSJ-gRNAs targeting the BSJ site (red arrow) were designed for each circRNA. nt, nucleotide. **b**, Evaluation of different Cas13-mediated KD on circRNAs with three gRNAs. Expression levels of *circPOLR2A* and *circRTN4*, and their cognate mRNAs were detected by quantitative PCR with reverse transcription (qRT-PCR) in 293FT cells. NT, non-targeting guide RNA. **c**, A paired control gRNA with partial sequences replaced by scrambled sequences for *circPOLR2A* or *circRTN4* did not guide RfxCas13d to affect circRNAs or mRNAs. **d**, Specific and robust KD of circRNAs by RfxCas13d–BSJ-gRNA in 293FT cells. **e**, KD of nine circRNAs by two RfxCas13d–BSJ-gRNAs or two position-matched shRNAs, as well as the expression of each cognate linear mRNA, was measured. $n=54$ biologically independent samples; transcript levels were normalized to *ACTB*. Data are presented as mean \pm s.d. **f**, Top, lengths and sequences of gRNA spacers flanking the *circPOLR2A* BSJ site; bases flanking the BSJ site were shown in red. Bottom, KD efficiencies of *circPOLR2A* and linear *POLR2A* by each BSJ-gRNA and RfxCas13d were detected by qRT-PCR. **g**, Plots of knockdown efficiencies of 54 guides for *circPOLR2A*, including 23 guides tiled across the BSJ and 31 guides tiled on the overlap region of *circPOLR2A* and linear *POLR2A*. **b–d,f**, All expression levels of RNAs were detected by qRT-PCR and were normalized to *ACTB*; means \pm s.d. were from three independent experiments. **b,d,e**, *P* values are by two-tailed Student's *t*-test.

were cultured for 30 days followed by gRNA enrichment and deep sequencing (Fig. 2b). The knockdown efficiency of three circRNAs remained unchanged after 30 days (Extended Data Fig. 3g). Deep

sequencing revealed that read distributions of two biologically independent experiments showed a relatively high correlation in HT29, HeLa and 293FT cells (Extended Data Fig. 3h). After 30 d of culture,



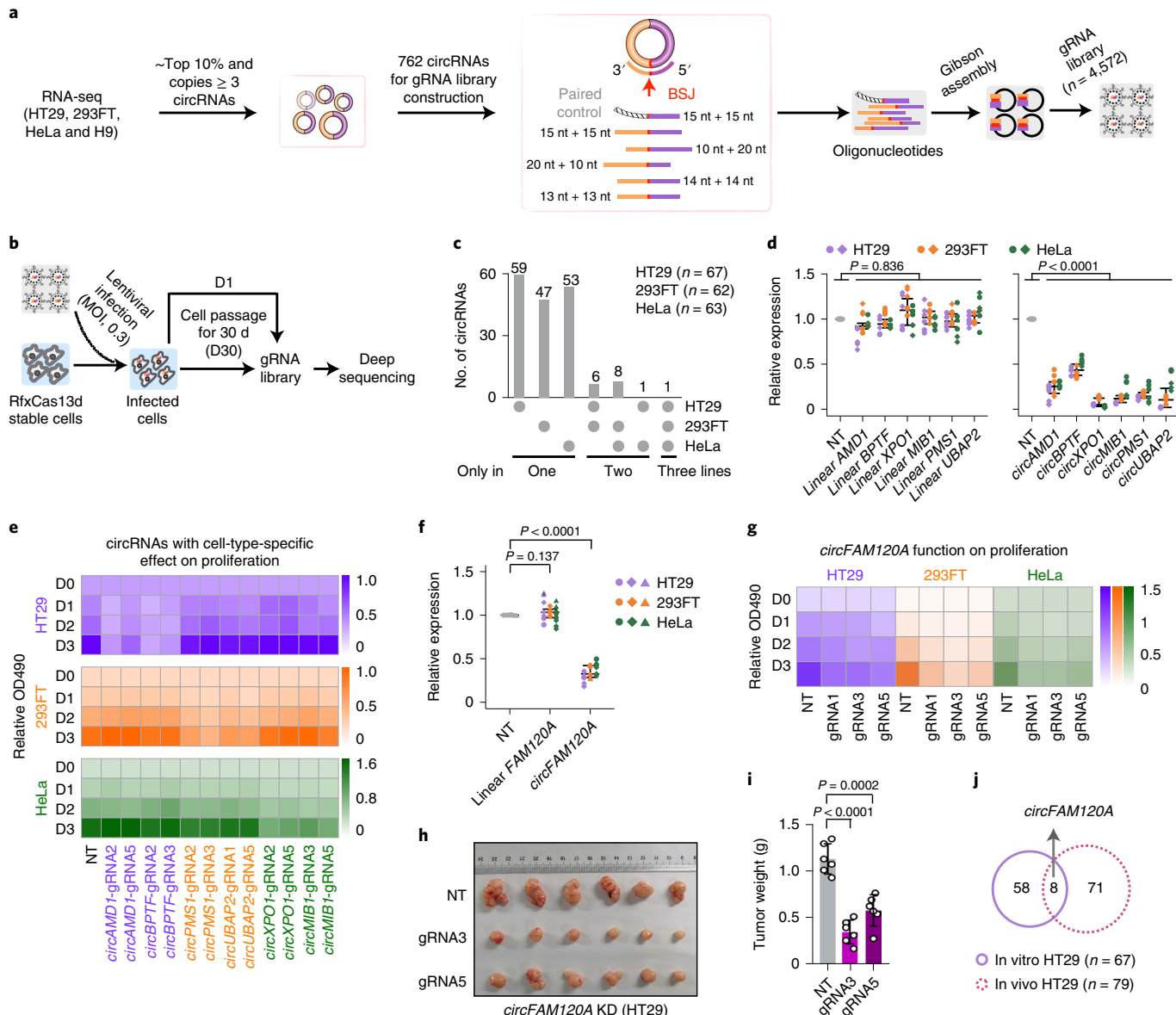


Fig. 2 | BSJ-gRNA library construction and circRNAs act in a cell-type-specific manner in cell proliferation. **a**, Schematic of gRNA library design and construction. One paired control gRNA ($n = 762$) and 5 BSJ-gRNAs (circRNA gRNAs, $n = 3,810$) were designed for each candidate circRNA. RNA-seq, RNA sequencing. **b**, A schematic of screen of circRNAs necessary for cell proliferation in HT29, 293FT and HeLa cells stably expressing RfxCas13d. MOI, multiplicity of infection. **c**, Analysis of circRNA hits that have potential impacts on cell growth by screens in HT29, 293FT and HeLa cells with CDCscreen score ≥ 2 , and with ≥ 2 negatively selected gRNAs with fold change (FC) ≤ 0.667 . **d**, KD of circRNAs with cell-type-specific growth effect by RfxCas13d-BSJ-gRNAs in HT29, 293FT and HeLa cells. Circles and diamonds in different colors indicate two gRNAs used for each RNA in different cells. $n = 18$ samples from 3 independent experiments. **e**, Cell-type-specific growth effect of circRNA candidates in HT29 (circAMD1, circBPTF), 293FT (circPMS1, circUBAP2) and HeLa cells (circXPO1, circMIB1) revealed by MTT cell-proliferation assays. Two gRNAs were examined in each case. **f**, KD of circFAM120A by RfxCas13d-BSJ-gRNAs in HT29, 293FT and HeLa cells. Circles, diamonds and triangles in different colors indicate three gRNAs used to target circFAM120A in different cells. $n = 27$ samples from three independent experiments. **g**, KD of circFAM120A by RfxCas13d-BSJ-gRNAs inhibited HT29, 293FT and HeLa cell growth and proliferation, as revealed by MTT cell proliferation assays. **h,i**, The image of tumors from nude mice injected subcutaneously with NT and circFAM120A-KD HT29 cells is shown in **h**; statistics on tumor weight are shown in **i**. $n = 6$ biologically independent samples. **j**, Overlap of circRNA candidates between *in vitro* (67) and *in vivo* (129) screens with CDCscreen score ≥ 2 , and with ≥ 2 negatively-selected gRNAs with FC ≤ 0.5 in HT29 cells. **d,f,i**, All expression levels of RNAs were detected by qRT-PCR and transcript levels were normalized to ACTB. **d,f,i**, P values are by two-tailed Student's *t*-test. Data are presented as means \pm s.d.

some gRNAs were obviously depleted compared with paired control gRNAs in each cell line (Extended Data Fig. 3i).

To identify circRNAs that are necessary for cell proliferation, we developed a Cas13d-mediated circRNA screen (CDCscreen) pipeline that adapts MAGeCK¹⁹ and additional filtering steps (Extended

Data Fig. 4a). Briefly, average normalized reads of negatively selected gRNAs obtained from RfxCas13d-BSJ-gRNA-treated cells at D1 and D30 were computed by the permutation test of MAGeCK¹⁹ to obtain P values for RfxCas13d-BSJ-gRNA-targeted circRNAs. Then, CDCscreen scores of expressed circRNAs in each cell line were

calculated by considering both *P* values and mean of gRNA fold change, which was obtained from normalized reads of negatively selected gRNAs targeting the same circRNAs between D30 and D1 treatments (Extended Data Fig. 4a, Methods and Supplementary Table 2). Only circRNAs with CDCscreen score ≥ 2 , ≥ 2 effective gRNAs and fold change ≤ 0.667 were identified as potential candidates for cell proliferation. A total of 67, 62 and 63 circRNAs were selected by CDCscreen in the HT29, 293FT and HeLa cell lines, respectively (Supplementary Table 3). Examples of identified circRNA candidates are shown in Extended Data Fig. 4b. Statistics for each gRNA and circRNA are listed in Supplementary Table 4, and an example is shown in Extended Data Fig. 4c. Importantly, $>50\%$ gRNAs of circRNA candidates were reduced by ≥ 1.5 -fold in all screens (Extended Data Fig. 4d), and all identified candidates had a false discovery rate <0.1 (ref. ²⁰) (Extended Data Fig. 4e).

We selected 9–10 circRNAs from circRNA candidates in each cell line for validation by RfxCas13d–BSJ-gRNA. We began with one BSJ-gRNA of each circRNA. The majority of circRNAs were successfully knocked down, with expected cell-growth inhibition in these cells (Extended Data Fig. 5a and Supplementary Table 5). Among them, *circHIPK3* and *circKLHL8* were reported to be necessary for cell proliferation by shRNA knockdown^{2,21}. To exclude potential off-targets on their parental genes, three BSJ-gRNAs targeting *circHIPK3* or *circKLHL8* were designed to deplete these circles and all exhibited high knockdown efficacy and retarded cell proliferation in HeLa and 293FT cells (Extended Data Fig. 5b–d). These phenotypes were unlikely to have resulted from off-target effects on their parental genes, which remained unchanged. Their suppression of cell proliferation could also be reproduced by shRNA-mediated knockdown (Extended Data Fig. 5e–g), even though two shRNAs targeting *circKLHL8* displayed distinct effects.

The majority of circRNA hits ($>80\%$) were unique to only one examined cell type (Fig. 2c and Extended Data Fig. 6a). This cell-type-specific mode of circRNAs on proliferation is unlikely due to different expression as they were expressed at similar levels in all three cell lines (Extended Data Fig. 6b,c). Further validation of circRNA hits by two CDCscreen-identified gRNAs (Fig. 2d) displayed consistent observations that knockdown of these circRNAs exhibited a cell-type-specific inhibition of cell growth (Fig. 2e). Of note, knockdown efficiency of different circRNAs by RfxCas13d–BSJ-gRNA in different cell lines was comparable.

RfxCas13d–BSJ-gRNA screens identify circRNAs that affect cell proliferation in vivo. Our screens and validations identified a previously unappreciated circRNA, *circFAM120A*, which is involved in proliferation of three examined cell lines (Fig. 2f,g and Extended Data Fig. 6d). This effect on cell growth was also seen by shRNA-mediated *circFAM120A* knockdown (Extended Data Fig. 6e–h). As RfxCas13d–BSJ-gRNAs could persistently knock down circRNAs (Extended Data Fig. 3g), we examined the effect of *circFAM120A* on cell proliferation in nude mice by introducing HT29 cells stably overexpressed with RfxCas13d and the control or BSJ-gRNAs targeting *circFAM120A*, which showed that *circFAM120A* is important for cell growth in vivo (Fig. 2h,i).

Next, to identify potential circRNA candidates involved in cell proliferation in vivo, we constructed a new library of BSJ-gRNAs that target 2,908 highly expressed circRNAs in 9 human cell lines (Extended Data Fig. 7a,b and Supplementary Table 6). This pool of circRNAs contains the most highly expressed circRNAs in examined human tissues (Extended Data Fig. 7c), representing a comprehensive pool for screening circRNAs in vivo. We carried out in vivo screens by transferring the BSJ-gRNA-library-infected RfxCas13d-HT29 cells into nude mice and obtained xenografts 22 d after injection (Extended Data Fig. 7d,e). Among 79 circRNA hits identified from in vivo screens selected by CDCscreen score ≥ 2 , and with ≥ 2 effective gRNAs and fold change ≤ 0.5 (Fig. 2j, Extended Data Fig. 7f,g and Supplementary Table 6), 8 hits overlapped with hits appeared in HT29 cells in vitro screens. *CircFAM120A* was among these overlapped candidates.

***CircFAM120A* is a common oncogenic circRNA that promotes cell growth by upregulating its parental-gene translation.** To gain insights into the mechanism of *circFAM120A* in cell proliferation, we performed transcriptomic analyses after *circFAM120A* knockdown by BSJ-gRNA or shRNA (Extended Data Fig. 8a). BSJ-gRNA-mediated knockdown showed a higher correlation with gene expression than did shRNAs (Extended Data Fig. 8b). Gene ontology of differentially expressed genes (DEGs) resulting from RfxCas13d–BSJ-gRNA-mediated *circFAM120A* knockdown revealed subtle transcriptome changes, but with an enrichment of altered genes involved in cell proliferation and apoptosis, including *EIF4EBP1*, *NUPR1* and *PCK2*, with reported oncogenic

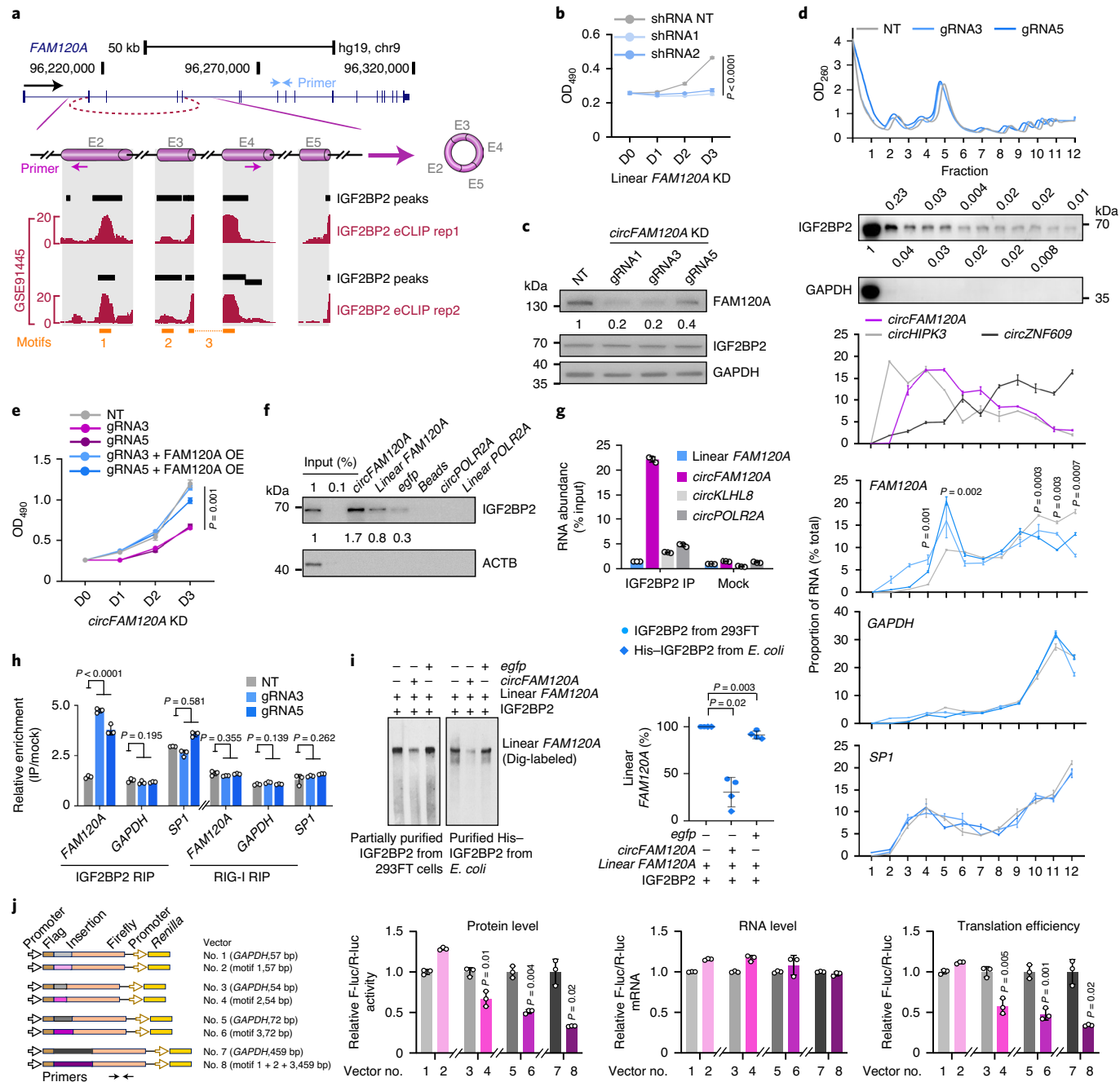
Fig. 3 | CircFAM120A promotes cell proliferation by preventing FAM120A mRNA from interacting with IGF2BP2 for efficient translation. **a**, Prediction of IGF2BP2-binding peaks in *circFAM120A*. Top, genomics locus and diagram of linear *FAM120A* and *circFAM120A* (shown as cylinders in magenta). Blue and magenta arrows indicate the location of the primer for linear *FAM120A* or *circFAM120A*, respectively. Bottom, IGF2BP2 binding peaks and wiggle-tracks of data from enhanced CLIP followed by sequencing (eCLIP-seq) in K562 cells (GEO, [GSE91445](#)) revealed that IGF2BP2 proteins were targeted on *circFAM120A*-producing circularized exons. IGF2BP2 binding motifs on *circFAM120A*-producing exons are shown as orange lines. **b**, KD of *FAM120A* mRNA by shRNAs inhibited 293FT cell proliferation, as revealed by MTT cell proliferation assays. OD_{490nm}, optical density at 480 nm. **c**, KD of *circFAM120A* by RfxCas13d–BSJ-gRNAs led to reduced *FAM120A* protein in 293FT cells, shown by western blot. **d**, Gradient traces of polysome profiling were shown (top). Fractions from NT cells were detected for IGF2BP2 and GAPDH by western blot, and *circFAM120A*, *circZNF609* and *circHIPK3* by qRT-PCR (middle). Fractions from NT or *circFAM120A* KD cells were detected for *FAM120A*, GAPDH and SP1 mRNAs by qRT-PCR (bottom). The y axis represents a percentage of specific RNAs in each fraction normalized to the total corresponding RNAs. **e**, Overexpression of *FAM120A* mRNA rescued the impaired cell proliferation in *circFAM120A* deficient cells, as revealed by MTT assays. **f**, *CircFAM120A* preferred to bind to IGF2BP2, revealed by biotin-labeled RNA pull-down assays followed by western blot to detect IGF2BP2 and ACTB. **g**, IGF2BP2 preferred to bind *circFAM120A*, compared with linear *FAM120A* or other circRNAs, revealed by IGF2BP2 RIP in 293FT cells. The abundance of RIP-enriched RNAs was measured by qRT-PCR. **h**, RIP assays of endogenous IGF2BP2 or RIG-I using corresponding antibodies in 293FT cells. RIG-I was used as a negative control for RIP assays. The abundance of mRNA was measured by qRT-PCR. **i**, Left, an equal amount of *circFAM120A* impaired *FAM120A* mRNA binding to IGF2BP2, which was immunoprecipitated from 293FT cells or purified from *E. coli*, shown by NB. Right, each dot represents quantification from in vitro competition assays at indicated conditions with two biological replicates. $n=4$ independent experiments. Data are presented as mean \pm s.d. Dig, digoxigenin. **j**, Left, schematic of a series of dual luciferase reporters. IGF2BP2 binding motifs on *circFAM120A* (motif 1, 2 and 3 in Fig. 3a) were inserted into the firefly luciferase (F-luc) mRNA. GAPDH sequences with corresponding lengths were used as controls in the same reporters. *Renilla* luciferase (R-luc) was used as an internal control to exclude potential influence resulted from transfection efficiency. Middle panels, F-luc and R-luc activities were detected by luciferin, and their mRNAs were detected by qRT-PCR. Right, insertion of IGF2BP2 binding motifs on *circFAM120A* into F-luc mRNA inhibited F-luc protein production. The translation efficiency of each reporter was calculated by luciferase activity normalized to luciferase mRNA level. **b,d,e,g,h,j**, Means \pm s.d. were from three independent experiments. **b,d,e,h-j**, *P* values are by two-tailed Student's *t*-test.

function involved in the AKT pathway^{22–25} (Extended Data Fig. 8c–g and Supplementary Table 7).

CircFAM120A is produced from *FAM120A* exon 2–5 (Fig. 3a) and is mainly localized in the cytosol (Extended Data Fig. 8h). Although predicted miRNA sites of AGO2 binding could be identified computationally from published photoactivatable ribonucleoside-enhanced cross-linking and immunoprecipitation (PAR-CLIP) datasets²⁶ (Extended Data Fig. 8i,j), ribonucleoprotein immunoprecipitation (RIP) assays with anti-AGO2 followed by examination of associated RNAs revealed undetectable interaction between *circFAM120A* and AGO2; *CDR1as* and *circCHIPK3* (refs. ^{21,26}) showed strong associations (Extended Data Fig. 8k). These results suggest that *circFAM120A* is unlikely to act as a miRNA sponge.

Given that *FAM120A* is an oncogenic gene related to the AKT pathway²⁷, we asked whether *circFAM120A* could promote cell

proliferation by regulating protein expression of its cognate *FAM120A* mRNA. First, knockdown of *FAM120A* mRNA by shRNAs showed an inhibitory effect on 293FT and HT29 cell proliferation (Fig. 3b and Extended Data Fig. 9a–d). Second, knockdown of *circFAM120A* by RfxCas13d-BSJ-gRNAs led to reduced *FAM120A* protein expression (Fig. 3c and Extended Data Fig. 9e) without affecting *FAM120A* mRNA level (Fig. 2f), indicating that this reduction resulted from inhibited translation of *FAM120A* mRNA. Consistent with this possibility, polysome profiling showed a shift of linear *FAM120A* mRNA from polyribosome to monoribosome fractions after *circFAM120A* knockdown (Fig. 3d and Extended Data Fig. 9f,g). As controls, distributions of *GAPDH* and *SP1* mRNAs remained unchanged. In addition, half-life detection showed unaffected stability of *FAM120A* protein after *circFAM120A* knockdown (Extended Data Fig. 9h). Third, transfection of *FAM120A*-overexpression vectors



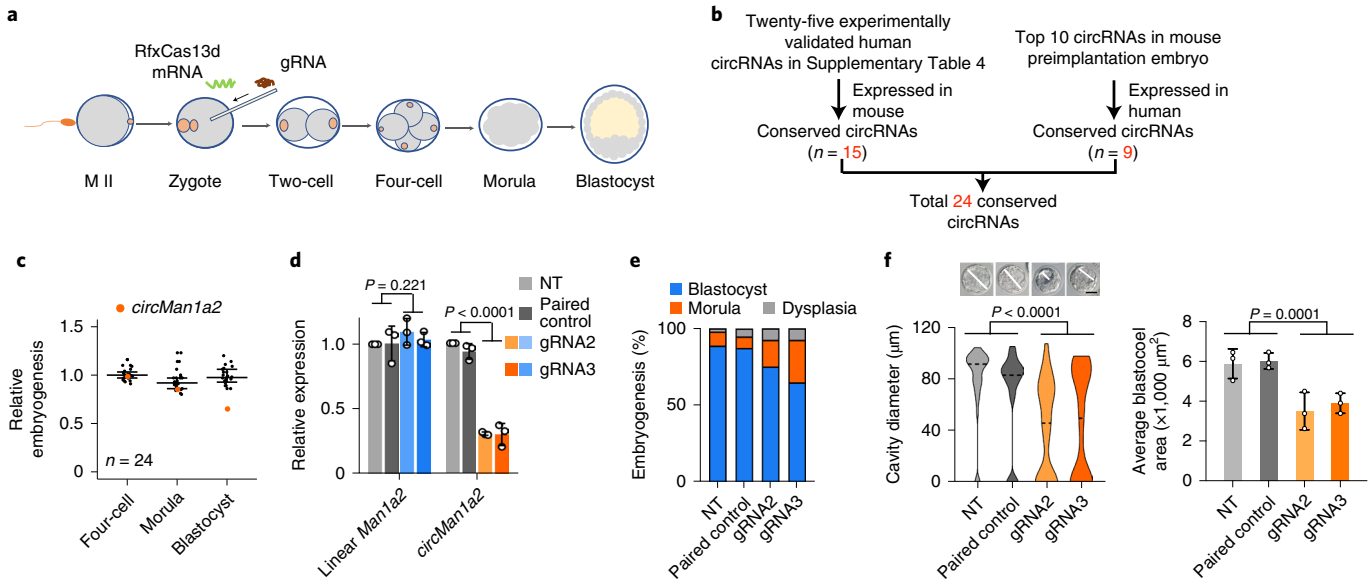


Fig. 4 | Screening circRNAs with functional potential during mouse preimplantation development with RfxCas13d-BSJ-gRNA. **a**, Schematic of RfxCas13d mRNA (green curve) and gRNA (brown curve) microinjection into mouse zygotes for RNA KD during preimplantation embryo development. **b**, A schematic workflow to show the strategy of selecting 24 circRNAs tested in the preimplantation development of mouse embryos. The expression data for circRNAs in mouse preimplantation embryo are from GEO GSE53386 (ref. ³³). **c**, Relative embryogenesis of 24 circRNA candidates KD by RfxCas13d-BSJ-gRNA during mouse preimplantation development. $n = 24$ circRNA candidates. Data are presented as means \pm s.d. **d**, Expression levels of circMan1a2 and linear Man1a2 were detected by qRT-PCR. All transcript levels were relative to Actb. **e**, KD of circMan1a2 led to reduced blastocyst formation 72 h after microinjection of RfxCas13d mRNA and the corresponding BSJ-gRNAs into mouse zygotes. **f**, Cavity diameter (left) and area (right) of blastocysts were measured at 72 h after microinjection of RfxCas13d mRNA and circMan1a2 BSJ-gRNAs into mouse zygotes. Brightfield images show the representative cavity diameter of blastocyst in each group (left). The blastocoel area was calculated as length \times width (right). Scale bar, 50 μm . **d,f**, Means \pm s.d. were from three independent experiments. **d,f**, P values are by two-tailed Student's *t*-test.

in *circFAM120A*-deficient cells rescued impaired cell proliferation (Fig. 3e). These results suggested that knockdown of *circFAM120A* inhibited cell growth by suppressing translation of its cognate linear mRNA.

CircFAM120A prevents FAM120A mRNA from binding to IGF2BP2, leading to efficient translation. To further explore how *circFAM120A* regulates *FAM120A* mRNA translation, we screened RBPs associated with the *circFAM120A*-producing locus from published eCLIP databases (<https://www.encodeproject.org/>) and identified insulin-like growth factor 2 mRNA binding protein 2 (IGF2BP2), a multiple functional RNA binding protein involved in cell proliferation by suppressing mRNA translation^{28,29} (Fig. 3a). IGF2BP2 is expressed at ~200,000 copies per cell with ~68% in the cytosol (Extended Data Fig. 9i–k). We speculated that *circFAM120A* might outcompete its cognate mRNA for IGF2BP2 binding, allowing the IGF2BP2-unbound *FAM120A* mRNA to be engaged with polyribosomes for translation.

To test this hypothesis, we performed a series of RNA pull-down and IGF2BP2 RIP assays. IGF2BP2 was strongly and specifically associated with *circFAM120A*, but not other examined circRNAs (Fig. 3f,g). Knockdown of *circFAM120A* enhanced linear *FAM120A* mRNA binding to IGF2BP2 but not to the control, RIG-I, in cells (Fig. 3h). Further, the IGF2BP2-unbound GAPDH and IGF2BP2-bound SP1 mRNAs remained unchanged, as were their mRNA distributions on polysomes (Fig. 3d), indicating this competition is specific between *circFAM120A* and *FAM120A* mRNA. In vitro competition assays with IGF2BP2 immunoprecipitated from 293FT cells or purified from *Escherichia coli* both showed that the equal amount of *circFAM120A* strikingly impaired *FAM120A* mRNA binding to IGF2BP2 (Fig. 3i). Of note, although the total *FAM120A* mRNA (~250–600 copies per cell) is more than tenfold

that of *circFAM120A* (~22 copies per cell) in examined cell lines (Extended Data Fig. 9j), their copies associated with IGF2BP2 were comparable (Extended Data Fig. 9l), indicating that *circFAM120A* binding to IGF2BP2 is accessible and preferential.

Polysome profiling in 293FT cells revealed distinct distributions of IGF2BP2, *circFAM120A* and *FAM120A* mRNAs (Fig. 3d and Extended Data Fig. 9m,n). In agreement with its inhibitory function in translation, cytoplasmic IGF2BP2 was mainly localized to ribosome-free fractions, where both circular and linear *FAM120A* RNAs were absent. Distinct from <5% IGF2BP2 and <10% of *FAM120A* mRNAs, the majority of *circFAM120A* presented in monoribosome fractions, resulting in a ~3:1 to ~5:1 stoichiometry between *FAM120A* mRNA and *circFAM120A* on monoribosomes. In contrast, >90% of *FAM120A* mRNAs were associated with polyribosomes.

How would the physiologically lower abundance of *circFAM120A* acquire higher interaction capability with IGF2BP2 than would linear *FAM120A* (Fig. 3g and Extended Data Fig. 9l)? IGF2BP2 is a reader protein of N⁶-methyladenosine (m⁶A) modification³⁰. *CircFAM120A* was m⁶A-modified³¹, and no m⁶A peak was found on the same *circFAM120A*-producing exons in poly(A) + *FAM120A* mRNA³², indicative of different m⁶A modifications in circular and linear *FAM120A*. We speculated that m⁶A-modified *circFAM120A* might enhance its binding preference to IGF2BP2. Consistent with this idea, in vitro assays confirmed that m⁶A modification promoted the interaction between *circFAM120A* and IGF2BP2 (Extended Data Fig. 9o) and enhanced its capability to compete with linear *FAM120A* for binding to IGF2BP2 at the physiological concentration (Extended Data Fig. 9p).

We further found that increased IGF2BP2 binding inhibited *FAM120A* mRNA translation by using a series of dual luciferase reporters (Fig. 3j) that contained IGF2BP2 binding motifs on

circFAM120A, but not *GAPDH* sequences with corresponding lengths. *Renilla* luciferase was used as an internal control to exclude potential influence resulted from transfection efficiency. These observations were unlikely to have resulted from transcription because firefly luciferase mRNA remained unaffected. Calculation of translation efficiency revealed that the increased IGF2BP2 binding suppressed mRNA translation. In agreement with these observations, knockdown of IGF2BP2 in *circFAM120A*-depleted cells rescued the reduction of *FAM120A* protein (Extended Data Fig. 9q), supporting a role for *circFAM120A* in promoting human cell proliferation by enhancing *FAM120A* mRNA translation via sequestering IGF2BP2.

Application of the RfxCas13d–BSJ–gRNA system to identify circRNAs important for mouse embryo development. It has been shown that circRNAs are abundant in mouse preimplantation embryos³³. However, it remains unknown whether any circRNA is important during development. To identify such circRNAs, we first explored whether the RfxCas13d–BSJ–gRNA system was applicable to mouse embryos. To do this, we microinjected purified RfxCas13d mRNAs and gRNAs targeting *Kras* and *Brg1* mRNAs into zygotes, followed by examining knockdown efficiency of each mRNA and defects in the preimplantation stage embryos (Fig. 4a). RfxCas13d–gRNAs displayed efficient knockdown of both *Kras* and *Brg1* mRNAs (Extended Data Fig. 10a). Knockdown of *Brg1*, but not *Kras*, led to reduced blastocyst formation (Extended Data Fig. 10b–d), as has been reported^{34,35}, suggesting the specificity and non-toxicity of using this system to study RNA function in mouse embryos.

Next, we applied this system to screen potentially functional circRNAs during preimplantation development of mouse embryos. We selected a pool of 24 mouse circRNAs containing 15 human circRNAs obtained from our screens (Fig. 2c) with mouse homolog circRNA expression in examined mouse cells and another 9 highly expressed and conserved circRNAs from mouse preimplantation embryos³³ (Fig. 4b). We confirmed their high expression during mouse preimplantation development (Supplementary Table 8). Initial screening was done by injecting RfxCas13d mRNA with 1 gRNA—each targeting 24 individual circRNAs into more than 30–50 mouse zygotes—and identified *circMan1a2* as a potential candidate important for mouse embryo preimplantation development (Fig. 4c and Supplementary Table 9).

CircMan1a2 is a conserved circRNA derived from exons 2–6 of its parental gene in mice and humans (Extended Data Fig. 10e). To exclude potential off-targets, one paired control and another BSJ–gRNA for *circMan1a2* were also tested. Consistent with results obtained in human cell lines (Fig. 1 and Extended Data Figs. 1 and 2), RfxCas13d with BSJ–gRNAs efficiently targeted *circMan1a2* for degradation with little effect on its cognate mRNA in mouse embryos (Fig. 4d). Importantly, the loss of *circMan1a2* in mouse zygotes led to aberrant embryonic development as shown by decreased blastocyst formation rate (Fig. 4e) and smaller blastocoel according to the diameter and area of cavity (Fig. 4f and Extended Data Fig. 10f). As controls, knockdown of other circRNAs had no detectable phenotype (Extended Data Fig. 10g–i and Supplementary Table 9). Of note, we observed some variations in phenotypes of RfxCas13d–gRNA-injected zygotes, which could result from different amounts of RNAs targeting *circMan1a2* being introduced into single zygotes even under parallel microinjection operations. Further implantation of these zygotes into pseudopregnant mice led to delayed postimplantation development (Extended Data Fig. 10j,k).

Discussion

Due to the complete sequence overlap, except BSJs, between back-spliced RNA circles and their linearly spliced RNA isoforms, functional studies of circRNAs have been impeded by the lack of

tools uniquely targeting these circles. We show that the RfxCas13d–BSJ–gRNA system achieves robust circRNA-specific knockdown without disturbing cognate mRNAs and that it is applicable at both individual and genome-wide levels. The Cas13 targeting poses a unique leverage to study LOF of circRNAs that are mainly derived from the middle exons of genes³⁶. At least two reasons account for this. First, the overall conformation of circRNAs is more stable and rigid than that of linear RNAs¹⁷. Once targeted by gRNA and Cas13, such rigid structures in circRNAs would continuously be targeted by this system; in a linear RNA, the highly dynamic and flexible folding status theoretically make it difficult for effective targeting continuously. Second, back-splicing efficiency is extremely slow, which is less than 1% of that of the canonical splicing in cells⁶. Once cleaved by Cas13, the newly produced circRNAs cannot compensate for the loss of circRNAs, leading to a consistent reduction of circRNAs by this system.

Screening circRNAs involved in cell growth suggests the cell-type-specific function of circRNAs, indicating that the majority of circRNAs may not play generic housekeeping roles but might act in a regulatory fashion in a cell-type-specific manner. Besides, our screens also identified one common oncogenic circRNA, *circFAM120A*, which promotes cell proliferation in vitro and in vivo by preventing *FAM120A* mRNA from binding the translation inhibitor IGF2BP2 (refs. ^{28,29}) for efficient translation. RfxCas13d–BSJ–gRNA screening also uncovered *circMan1a2* with regulatory potential in mouse embryo preimplantation development with an unknown mechanism. Future generation of circRNA LOF mouse models without affecting parental mRNA expression will be a necessity to prove the physiological importance of *circMan1a2*. Nevertheless, application of the RfxCas13d–BSJ–gRNA system will likely enable the discovery of functional circRNAs in both physiological and pathological conditions.

Online content

Any methods, additional references, Nature Research reporting summaries, source data, extended data, supplementary information, acknowledgements, peer review information; details of author contributions and competing interests; and statements of data and code availability are available at <https://doi.org/10.1038/s41592-020-01011-4>.

Received: 27 July 2020; Accepted: 26 October 2020;

Published online: 07 December 2020

References

- Li, X., Yang, L. & Chen, L. L. The biogenesis, functions, and challenges of circular RNAs. *Mol. Cell* **71**, 428–442 (2018).
- Chen, S. et al. Widespread and functional RNA circularization in localized prostate cancer. *Cell* **176**, 831–843(2019).
- Guarnerio, J. et al. Oncogenic role of fusion-circRNAs derived from cancer-associated chromosomal translocations. *Cell* **166**, 1055–1056 (2016).
- Legnini, I. et al. Circ-ZNF609 is a circular RNA that can be translated and functions in myogenesis. *Mol. Cell* **66**, 22 (2017).
- Piwecka, M. et al. Loss of a mammalian circular RNA locus causes miRNA deregulation and affects brain function. *Science* **357**, eaam8526 (2017).
- Zhang, Y. et al. The biogenesis of nascent circular RNAs. *Cell Rep.* **15**, 611–624 (2016).
- Xia, P. et al. A circular RNA protects dormant hematopoietic stem cells from DNA sensor cGAS-mediated exhaustion. *Immunity* **48**, 688–701 e687 (2018).
- Abudayyeh, O. O. et al. C2c2 is a single-component programmable RNA-guided RNA-targeting CRISPR effector. *Science* **353**, aaf5573 (2016).
- East-Seletsky, A. et al. Two distinct RNase activities of CRISPR-C2c2 enable guide-RNA processing and RNA detection. *Nature* **538**, 270–273 (2016).
- Shmakov, S. et al. Discovery and functional characterization of diverse class 2 CRISPR–Cas systems. *Mol. Cell* **60**, 385–397 (2015).
- Konermann, S. et al. Transcriptome engineering with RNA-targeting type VI-D CRISPR effectors. *Cell* **173**, 665–676 e614 (2018).
- Abudayyeh, O. O. et al. RNA targeting with CRISPR–Cas13. *Nature* **550**, 280–284 (2017).

13. Yan, W. X. et al. Cas13d Is a compact RNA-targeting type VI CRISPR effector positively modulated by a WYL-domain-containing accessory protein. *Mol. Cell* **70**, 327 (2018).
14. Cox, D. B. T. et al. RNA editing with CRISPR–Cas13. *Science* **358**, 1019–1027 (2017).
15. Hansen, T. B. et al. miRNA-dependent gene silencing involving Ago2-mediated cleavage of a circular antisense RNA. *EMBO J.* **30**, 4414–4422 (2011).
16. Chen, G. W., Shi, Y. T., Zhang, Y. & Sun, J. Y. CircRNA_100782 regulates pancreatic carcinoma proliferation through the IL6-STAT3 pathway. *Oncotarget* **10**, 5783–5794 (2017).
17. Liu, C. X. et al. Structure and degradation of circular RNAs regulate PKR activation in innate immunity. *Cell* **177**, 865–880 e821 (2019).
18. Zhang, X. O. et al. Diverse alternative back-splicing and alternative splicing landscape of circular RNAs. *Genome Res* **26**, 1277–1287 (2016).
19. Li, W. et al. MAGeCK enables robust identification of essential genes from genome-scale CRISPR/Cas9 knockout screens. *Genome Biol.* **15**, 554 (2014).
20. Liu, S. J. et al. CRISPRi-based genome-scale identification of functional long noncoding RNA loci in human cells. *Science* **355**, aah7111 (2017).
21. Zheng, Q. P. et al. Circular RNA profiling reveals an abundant circHIPK3 that regulates cell growth by sponging multiple miRNAs. *Nat. Commun.* **7**, 11215 (2016).
22. Lee, M., Kim, E. J. & Jeon, M. J. MicroRNAs 125a and 125b inhibit ovarian cancer cells through post-transcriptional inactivation of EIF4EBP1. *Oncotarget* **7**, 8726–8742 (2016).
23. Mu, Y. C. et al. NUPR1 maintains autolysosomal efflux by activating SNAP25 transcription in cancer cells. *Autophagy* **14**, 654–670 (2018).
24. Vincent, E. E. et al. Mitochondrial phosphoenolpyruvate carboxykinase regulates metabolic adaptation and enables glucose-independent tumor growth. *Mol. Cell* **60**, 195–207 (2015).
25. Wallin, J. J. et al. Nuclear phospho-Akt increase predicts synergy of PI3K inhibition and doxorubicin in breast and ovarian cancer. *Sci. Transl. Med.* **2**, 48ra66 (2010).
26. Memczak, S. et al. Circular RNAs are a large class of animal RNAs with regulatory potency. *Nature* **495**, 333–338 (2013).
27. Bartolome, R. A. et al. IL13 receptor α 2 signaling requires a scaffold protein, FAM120A, to activate the FAK and PI3K pathways in colon cancer metastasis. *Cancer Res* **75**, 2434–2444 (2015).
28. Li, Z. et al. An HMGA2-IGF2BP2 axis regulates myoblast proliferation and myogenesis. *Dev. Cell* **23**, 1176–1188 (2012).
29. Dai, N. et al. IGF2BP2/IMP2-deficient mice resist obesity through enhanced translation of Ucp1 mRNA and other mRNAs encoding mitochondrial proteins. *Cell Metab.* **21**, 609–621 (2015).
30. Huang, H. et al. Recognition of RNA N⁶-methyladenosine by IGF2BP proteins enhances mRNA stability and translation. *Nat. Cell Biol.* **20**, 285–295 (2018).
31. Zhou, C. et al. Genome-wide maps of m6A circRNAs identify widespread and cell-type-specific methylation patterns that are distinct from mRNAs. *Cell Rep.* **20**, 2262–2276 (2017).
32. Batista, P. J. et al. m⁶A RNA modification controls cell fate transition in mammalian embryonic stem cells. *Cell Stem Cell* **15**, 707–719 (2014).
33. Fan, X. et al. Single-cell RNA-seq transcriptome analysis of linear and circular RNAs in mouse preimplantation embryos. *Genome Biol.* **16**, 148 (2015).
34. Bultman, S. et al. A Brg1 null mutation in the mouse reveals functional differences among mammalian SWI/SNF complexes. *Mol. Cell* **6**, 1287–1295 (2000).
35. Bultman, S. J. et al. Maternal BRG1 regulates zygotic genome activation in the mouse. *Genes Dev.* **20**, 1744–1754 (2006).
36. Zhang, X. O. et al. Complementary sequence-mediated exon circularization. *Cell* **159**, 134–147 (2014).

Publisher's note Springer Nature remains neutral with regard to jurisdictional claims in published maps and institutional affiliations.

© The Author(s), under exclusive licence to Springer Nature America, Inc. 2020

Methods

Cell culture. HT29, HeLa and 293FT cells were purchased from the American Type Culture Collection (ATCC; <http://www.atcc.org>) or Thermo Fisher, respectively, and were originally authenticated using STR profiling. HT29 cells were maintained in RPMI 1640, HeLa (human female origin) and 293FT cells (human fetus origin) were maintained in DMEM, and all were supplemented with 10% FBS and 0.1% penicillin–streptomycin. We maintained cell lines at 37 °C in a 5% CO₂ cell-culture incubator and tested all cell lines routinely to exclude mycoplasma contamination.

Plasmid construction and transfection. To construct Cas13 expression vectors, human codon-optimized DNA sequences of LwaCas13a, PspCas13b, PguCas13b, RanCas13b, EsCas13d, AdmCas13d and RfxCas13d were synthesized in Genscript. Then, the DNA sequences were amplified by DNA Polymerase High Fidelity (TransGen) and cloned into the p23-phage vector containing sequences for a C-terminal-fused msfGFP and a Flag tag. DNA sequence of RfxCas13d was further cloned into the p23-phage vector containing sequences for a C-terminal fused mCherry and a Flag tag (p23-RfxCas13d-mCherry-Flag). To construct gRNA expression vectors, DNA sequences for gRNAs were synthesized and cloned into PUC19 or pLKO.1-TRC containing direct repeats of each corresponding Cas13. To construct shRNA expression vectors, DNA sequences of shRNAs were synthesized and cloned into the pLKO.1-TRC vector. To construct luciferase reporters, DNA sequences of IGF2BP2 binding motifs of *circFAM120A*-producing exons were inserted into firefly luciferase mRNA. As controls, GAPDH sequences with corresponding lengths were inserted into firefly luciferase mRNA. To construct IGF2BP2 vector for purification, DNA sequences of IGF2BP2 was cloned into pET-28a vector containing sequences for an amino-terminal-fused His tag (His-IGF2BP2). All constructed vectors were transformed into Trelief 5x Chemically Competent Cell (Tsingke Biological Technology) for plasmid replication and amplification. All gRNAs and shRNAs are listed in Supplementary Table 10.

Plasmid transfection was carried out using Lipofectamine 3000 Reagent (ThermoFisher) according to manufacturer's protocols. About 80–90% transfection efficiency was achieved in HeLa and 293FT cells. Cells were collected 48 h after transfection for further RNA expression analysis.

Lentivirus production and cell infection. For the production of lentiviral particles, 293FT cells were cultured to reach 5×10^6 in a 10-cm dish and then cotransfected with an expression vector of interest (~10 µg), the psPAX2 vector (~7.5 µg) and the pMD2.G vector (~3 µg). To collect viral particles, the supernatant of cultured 293FT cells was passed through Millipore Millex-GP Filter Unit with 0.22-mm pore size, individually at 48 h and 72 h after transfection. The viral particles were enriched by Lenti-Concentin Virus Precipitation Solution (ExCell Bio) and then resuspended with 1 ml PBS containing 0.1% BSA. These resuspended viral particles were further aliquoted and stored at -80 °C before use. Lentivirus infection was performed by culturing cells (HeLa, 293FT or HT29 in this study) with corresponding medium containing 10 µl suspended lentiviral particles and 5 mg ml⁻¹ polybrene (Sigma). To increase efficiency for better knockdown effects, infected cells were further treated with puromycin (1 µg ml⁻¹) for several days.

Generation of RfxCas13d-expressed stable cell lines.

p23-RfxCas13d-mCherry-Flag vector was infected into HeLa, 293FT and HT29 cells by lentivirus for stable cell line generation. RfxCas13d-expressed stable cell lines were obtained from single clones with red fluorescence, which were validated by WB with anti-Flag antibodies.

RNA isolation and qRT-PCR. To purify total RNAs from cultured cells, TRIzol (Life Technologies) was used according to the manufacturer's protocol. After TRIzol purification, extracted RNAs were first treated with DNase I (Ambion, DNA-free kit) to remove possible DNA contamination and then were reverse transcribed to produce cDNAs by using the PrimeScript RT Reagent Kit (Takara). These cDNAs were then used for qPCR to evaluate gene expression with the primers listed in Supplementary Table 10. The expression of ACTB was used as an internal control for normalization.

Northern blotting. Northern blotting was performed to examine RNA levels of targeted genes by using DIG Northern Starter Kit (Roche). Briefly, 5 µg of total RNAs or purified RNAs binding to IGF2BP2 in *in vitro* assays were resolved on denaturing urea PAGE. After transferred to nylon membrane (Roche), RNAs were ultraviolet cross-linked and then hybridized with specific Dig-labeled riboprobes that were prepared by using RiboMAX Large Scale RNA Production Systems (Promega). Primers for NB probes to detect *circPOLR2A* and *circFAM120A* are listed in Supplementary Table 10.

Western blotting. Cells were collected after treatment and were resuspended in lysis buffer (1% NP-40, 0.5% sodium deoxycholate, 0.1% SDS, 150 mM NaCl, 50 mM Tris and 1× protease inhibitor cocktail, pH 8.0) for 10 min. After centrifugation, supernatants containing soluble proteins were resolved on polyacrylamide gel with 10% SDS and analyzed by western blot with anti-Flag (Sigma, 1:1,000 dilution), anti-FAM120A (Abcam, 1:1,000 dilution), anti-IGF2BP2

(Abcam, 1:1,000 dilution), anti-GAPDH (GNI, 1:2,000 dilution), anti-RIG-I (ABclonal, 1:1,000 dilution) or anti-ACTB (Sigma, 1:5,000 dilution) antibodies.

Cell proliferation assay. To validate the effect of circRNA on cell proliferation, BSJ-gRNAs targeting the BSJ site of each circRNA were infected into HeLa, 293FT or HT29 cell lines that stably expressed RfxCas13d. Cells with specific circRNA-knockdown were obtained by puromycin (1 µg ml⁻¹) selection. Knockdown efficiencies of circRNAs by RfxCas13d-BSJ-gRNAs or shRNAs were measured prior to performing cell proliferation assays.

Cell proliferation was detected by an MTT assay that measures OD₄₉₀ according to CellTiter 96 AQueous One Solution Cell Proliferation Assay (Promega), or by Envision Multimode Plate Reader (PerkinElmer) that measures the occupied surface area of cells to indicate confluence. We seeded 5×10^3 HeLa, 293FT or HT29 cells into each well of 96-well dishes, then cultured these at 37 °C in a 5% CO₂ cell-culture incubator until the indicated time points. Cell proliferation at D0 was detected after cells were seeded for 5 h to allow them to attach to the plate. Live cells at D1, D2 and D3 were detected by MTT or by Envision Multimode Plate Reader. Data were normalized to the value at D0.

Subcutaneous xenograft tumor model. All animal procedures were performed according to the ethical guidelines of the Chinese Academy of Sciences (CAS) Center for Excellence in Molecular Cell Science. With free access to food and water, temperature at 20–25 °C and humidity at 50 ± 10%, mice were maintained under a 12 h/12 h light-dark cycle. For assay of the formation of subcutaneous xenograft tumors, 4- to 5-week-old male BALB/c-nu/nu mice (six mice per group) were injected subcutaneously with 1×10^6 HT29 cells. When mice were euthanized, the tumors were collected and weighed.

Subcellular fractionation. With slight modifications, nuclear and cytoplasmic fractionation of cells was carried out as previously described³⁷. In brief, after washing with PBS, 3×10^6 cells were collected at room temperature by centrifugation at 200g for 2 min, and then resuspended in 300 µl lysis buffer (1% NP-40, 0.5% sodium deoxycholate, 5 mM EDTA, 1 mM DTT, 1 mM PMSF, 2 mM RVC, 15% glycerol and 1× protease inhibitor cocktail) on ice for 5 min. Cell lysates were centrifuged at 4 °C at 4,000g for 1 min to collect the supernatant through cytoplasmic fractionation after the membranes of most of cells were disrupted by an optical microscope. After rinsing, the precipitated pellet was resuspended in 300 µl lysis buffer and further treated with sonication and centrifugation at 4 °C at 12,000g for 10 min to save the supernatant as nuclear fractionation.

In vitro RNA transcription, circularization and purification. With slight modifications, *in vitro* RNA transcription (IVT) assays were performed as previously described¹⁷. Briefly, template DNAs were PCR-amplified by PrimeStar DNA polymerase (Takara) and then used for *in vitro* transcription by T7 RNA polymerase (Novoprotein) with dNTPs. To produce 5'-monophosphate RNA for circularization, GMP was supplemented in the IVT at a concentration of 2 mM. For synthesis of m⁶A-labeled or biotin-labeled RNAs, m⁶A or biotin-labeled uridine was individually added into the reaction mixture at 37 °C for 2 h. After DNase I treatment to remove template DNAs, IVT-RNAs were precipitated with ethanol and resuspended in RNase-free water after rinsing.

To generate circular RNAs, 50 µg of IVT-RNAs were incubated with T4 RNA ligase 2 (NEB) at 16 °C overnight, and then treated with RNase R as previously described¹⁶. Circularized RNAs were then precipitated with ethanol and resuspended in RNase-free water after rinses. Both IVT linear and circularized RNAs were resolved on denaturing urea PAGE, and were stained by ethidium bromide (EB) for visualization. EB-stained bands that correspond to circularized RNAs were excised and purified for subsequent analyses.

RNA pull-down. Biotinylated linear or circular RNAs were denatured at 65 °C for 5 min in PA buffer (pH 7.5 10 mM Tris HCl, 10 mM MgCl₂ and 100 mM NH₄Cl) and then cooled down to room temperature before use. Cell lysates were prepared from 5×10^6 cells, which were resuspended in 1 ml binding buffer (pH 7.0 10 mM HEPES, 50 mM KCl, 1 mM EDTA, 1 mM DTT, 10% glycerol, 0.5% Triton X-100 and 0.5 mg ml⁻¹ heparin) for sonication. After sonication, cell lysates were centrifuged at 4 °C with 12,000g for 10 min to collect the supernatants, which were precleared with Streptavidin Dynabeads (Invitrogen) at room temperature for 30 min. The supernatants were then incubated with pretreated RNAs for 30 min and Streptavidin Dynabeads (Invitrogen) for 10 min. RNA-associated proteins were pulled down with beads and then subjected to western blot for validation.

RNA competition assay. Purified *circFAM120A* with or without m⁶A modification and Dig-labeled linear *FAM120A* were individually denatured at 65 °C for 5 min in PA buffer (pH 7.5 10 mM Tris HCl, 10 mM MgCl₂ and 100 mM NH₄Cl) and then cooled down to room temperature slowly. Together with 1 pmol folded Dig-labeled linear *FAM120A*, 1 or 0.25 pmol *circFAM120A* with or without m⁶A modification was added into 0.3 ml binding buffer (pH 7.0 50 mM HEPES, 150 mM NaCl, 10 mM MgCl₂, 0.1 mM DTT, 0.5 mM PMSF and 2 mM RVC) containing 1 pmol IGF2BP2 protein immunoprecipitated from 293FT cells or purified from *E. coli*.

Dig-labeled linear *FAM120A* binding with IGF2BP2 was collected and extracted by TRIzol (Life Technologies). Northern blotting was used to examine the relative binding abundance of Dig-labeled linear *FAM120A* in the reactions.

Circular RNA binding assay. Purified *circFAM120A* with or without m⁶A modification was denatured at 65 °C for 5 min in PA buffer (pH 7.5 10 mM Tris HCl, 10 mM MgCl₂ and 100 mM NH₄Cl) and then cooled down to room temperature slowly. For the binding assay, 1 pmol folded *circFAM120A* with or without m⁶A modification was added into 0.3 ml binding buffer (pH 7.0 50 mM HEPES, 150 mM NaCl, 10 mM MgCl₂, 0.1 mM DTT, 0.5 mM PMSF and 2 mM RVC) containing 1 pmol His-IGF2BP2 proteins purified from *E. coli*. *CircFAM120A* bound with His-IGF2BP2 was collected by Ni beads and extracted by TRIzol (Life Technologies). Northern blotting was used to examine the relative binding abundance of *circFAM120A* with or without m⁶A modification.

Ribonucleoprotein immunoprecipitation. After being rinsed with ice-cold PBS, cells growing in 15-cm dishes were collected at 4 °C by centrifugation at 200g for 5 min, resuspended in 1 ml RIP buffer (pH 8.0 50 mM Tris, 150 mM NaCl, 1 mM PMSF, 2 mM VRC, 0.5% IgEpal and 1× protease inhibitor cocktail) and subjected to gentle sonication three times. Cell lysates were then centrifuged at 4 °C with 12,000g for 15 min to collect the supernatants, which were precleared with 15 ml Dynabeads Protein G (Invitrogen) to block non-specific binding. A series of antibodies, anti-AGO2 (Sigma, with final concentration at 2 µg/mg of lysates), anti-IGF2BP2 (Abcam, with final concentration at 2 µg/mg of lysates) or anti-RIG-I (Abclonal, with final concentration at 2 µg mg⁻¹ of lysates) antibodies, were individually used for RIP assays with precleared lysates and Dynabeads Protein G at 4 °C for 2 h. After being washed with high-salt buffer 3 times and with the RIP buffer 2 times, proteins and RNAs that were associated with beads were eluted with the elution buffer (pH 6.8 100 mM Tris, 10 mM EDTA and 4% SDS) at room temperature. One-third of the eluted sample was directly used for western blotting to validate associated protein components. The remaining sample was further treated with TRIzol (Life technologies) for RNA purification and then subject to RNA quantification by qRT-PCR with primers listed in Supplementary Table 10.

Polysome fractionation. About 2 × 10⁷ cells with or without *circFAM120A* KD were first treated with cycloheximide (100 µg ml⁻¹) for 15 min and then lysed with 500 µl lysis buffer (pH 7.4 20 mM Tris, 15 mM MgCl₂, 200 mM KCl, 1 mM DTT, 100 µg ml⁻¹ cycloheximide, 1 mg ml⁻¹ heparin, 40 U ml⁻¹ RNasin (Promega) and 1% Triton X-100). Supernatants were collected at 4 °C by centrifugation at 12,000g for 10 min, and then loaded onto 5–50% sucrose gradients for fractionation by ultracentrifugation. Linear sucrose gradients were prepared with a Gradient Master (Biocomp), according to manufacturer's suggestions, and the ultracentrifugation was performed with a SW41 rotor (Beckman) at 4 °C at 36,000g for 2.5 h. Ribosome distribution on the sucrose gradients was recorded at 254 nm by BIOCOMP Piston Gradient Fractionator equipped with BIO-RAD ECONO UV Monitor.

Protein purification. His-IGF2BP2 vector was transformed into *E. coli* Tranetta (DE3) chemically competent BL21 (Transgen Biotech, CD801) cells. A single transformed colony was selected and then cultured in 5 ml LB medium (contained 100 µg l⁻¹ kanamycin) at 37 °C at 300 r.p.m. and left overnight in an incubator shaker. The medium was diluted about 100-fold into 11 fresh LB medium (contained 100 µg l⁻¹ kanamycin) and was continuously cultured until its OD₆₀₀ reached 0.6–0.8. IPTG was then added into the LB culture medium, with a final concentration at 0.5 mM, to induce protein expression at 16 °C by overnight shaking at 180 r.p.m. After that, His-IGF2BP2-transfected *E. coli* cells were collected and then lysed in lysis buffer (pH 7.5–8.0 20 mM Tris HCl, 500 mM NaCl, 12 mM β-mercaptoethanol, 0.5 mM PMSF and 1 mg ml⁻¹ lysozyme) at 4 °C for 30 min. Cell lysates were fragmented at 4 °C by high-pressure homogenizer (Ultrahigh Pressure Cell Crusher UH-06; Union-Biotech). Then, the cell fragments were centrifuged at 4 °C at 12,000g for 30 min, and the Ni sepharose beads (GE Healthcare, 17-5318-01) were incubated with supernatant at 4 °C for 2 h. After being washed twice with washing buffer (pH 7.5–8.0 20 mM Tris HCl, 500 mM NaCl, 20 mM imidazole and 0.5 mM PMSF), IGF2BP2 proteins that were associated with beads were eluted by the elution buffer (pH 7.5–8.0 20 mM Tris HCl, 500 mM NaCl, 250 mM imidazole and 0.5 mM PMSF), further purified by the gel filtration chromatography (Superdex-200; GE Healthcare) and then collected with storage buffer (pH 7.5–8.0 20 mM Tris HCl, 500 mM NaCl, 0.1 mM PMSF and 3% glycerol).

Luciferase reporter assay. One microgram of reporter plasmids with insertion of GAPDH and *FAM120A* DNA sequences were transfected into 293FT cells in a six-well plate using Lipofectamine 3000 Reagent (Invitrogen). At 24 h post-transfection, transfected 293FT cells were re-seeded into a 96-well plate (5 × 10⁴ cells in each well) in 3 replicates. At 24 h after, cells in the 96-well plate were assayed by the DualGlo Luciferase Assay System (Promega), according to the manufacturer's instructions. F-luc activity was normalized to that of R-luc to evaluate the translation of individual reporters.

Determination of *FAM120A* protein stability. To determine the *FAM120A* protein stability, equal numbers of control or *circFAM120A* KD 293FT cells were

plated into 12-well plates; 12 h after, cells were treated with 50 µg ml⁻¹ CHX for the indicated times. The protein levels were determined by western blot, and the intensity of the signals was quantified by ImageJ (v1.52).

Zygote injection and in vitro embryo culture. Eight-week-old female B6D2F1 mice (C57BL/6 × DBA/2) were superovulated and mated with male B6D2F1 mice. Fertilized embryos were then collected from oviducts after 21–23 h. By using a Femtojet microinjector (Eppendorf) with constant flow settings, pre-mixed RfxCas13d mRNAs (100 ng µl⁻¹) and gRNA (100 ng µl⁻¹) were injected into the cytoplasm of fertilized embryos in a droplet of HEPES-CZB medium containing 5 µg µl⁻¹ cytosolic calasin B (Sigma). After injection, fertilized embryos were further cultured at 37 °C in KSOM medium with amino acids under 5% CO₂ in air until the hatching blastocyst stage by 4 d.

Embryo transfer and cesarean section. After injection, fertilized embryos were cultured in KSOM medium with amino acids until they reached two-cell stage. In total, 12 two-cell mouse embryos were transferred into oviducts of E0.5 ICR recipients, which were pseudopregnant mice mated with vasectomized male ICR mice one day before. Recipient mothers were euthanized at 7.5 d of gestation, and embryos were immediately removed from the uterus.

Screening for circRNAs with functional potential using the RfxCas13d-gRNA library. The step-by-step protocol of gRNA library design and construction and screening for functional circRNAs on cell proliferation is provided as a Supplementary Protocol and is available at Protocol Exchange³⁸. There are two gRNA libraries that target BSJ sites of either 762 (Supplementary Table 1) or 2,908 circRNAs (Supplementary Table 6). The library targeting 762 or 2,908 circRNAs was applied for the *in vitro* screens (239FT, HeLa and HT29 cell lines) or *in vivo* screen (HT29 cell line), respectively.

Computational analysis of circRNA screens. A computational pipeline was developed to identify negatively selected circRNAs that promote cell proliferation based on Cas13d-mediated circRNA screen (CDCscreen), by adapting MAGeCK (v0.5.9.2)¹⁹ with additional filtering steps. gRNA enrichment and deep sequencing datasets were obtained from two biological replicates treated with RfxCas13d/BSJ-gRNA library at D1 and D30, respectively. Adapters at 3' end and 5' end in the raw paired-end sequencing datasets were removed by cutadapt (v1.16) using the following adapter sequences:

R1: -a TTTTTAACTGGCGTAACTAGATCT -m 15,
-g CCCTACCAACTGGTCGGGGTTGAAAC -m 15;
R2: -a GTTCAAACCCCGACCAGTTGGTAGGG -m 15,
-g AGATCTAGTTACGCCAACGCTTAAAAAA -m 15.

After removing adapters at 3' and 5' ends, processed reads were aligned to gRNA library sequences with Bowtie (v1.1.2, parameters: -v 3 -m 1 -k 1), and only uniquely mapped reads were obtained for gRNA enrichment.

Uniquely mapped reads for each unique gRNA were normalized as following formula:

$$\text{normalized reads per gRNA} = \frac{\text{reads per gRNA}}{\text{total reads for all gRNAs in samples}} \times 10^5 + 1$$

After assessment with Pearson correlation coefficient to show correlation between two biological replicates, average normalized reads of each gRNA from two biological replicates were used for subsequent analysis. Average normalized reads of negatively selected gRNAs obtained from RfxCas13d-BSJ-gRNA-treated cells at D1 and D30 were computed by the permutation test of MAGeCK¹⁹ to obtain *P* values of RfxCas13d-BSJ-gRNA-targeted circRNAs. Effects of RfxCas13d-BSJ-gRNA-targeted circRNAs on cell proliferation were then evaluated by the following equation:

$$\text{CDCscreen score} = \text{scale}[-\log_{10}(P)] + \text{scale}[\log_2(\text{Mean of gRNA fold change})]$$

where "mean of gRNA fold change (FC)" was obtained from normalized reads of negatively selected gRNAs targeting the same circRNAs between D30 and D1 treatments. Only expressed circRNAs with FPBcirc > 0 in each type of examined cell line were calculated.

Next, we calculated the empirical false discovery rate (FDR) of each circRNA in each screening. Briefly, negative control circRNAs were generated by randomly sampling five non-targeting paired-control gRNAs for each circRNA from 762 non-targeting paired-control gRNAs, to match each true circRNA that contains five BSJ-gRNAs in the library (Fig. 2a). Then, CDCscreen scores of all negative control circRNAs and true circRNAs were calculated by the pipeline in Extended Data Fig. 4a. After obtaining the CDCscreen scores of negative control circRNAs and true circRNAs, these scores were used to calculate empirical FDR as reported²⁰. Finally, circRNA candidates with potential effects on cell proliferation were selected by CDCscreen score ≥ 2, ≥ 2 negatively selected gRNAs with FC ≤ 0.667 and FDR of each circRNA < 0.1 (Supplementary Table 3). Similarly, circRNA candidates with potential effects on cell proliferation *in vivo* (Extended Data Fig. 7a) were selected by CDCscreen score ≥ 2, ≥ 2 negatively selected gRNAs with FC ≤ 0.5 and FDR of each circRNA < 0.1 (Supplementary Table 6).

Polyadenylated RNA library preparation, deep sequencing and analysis. Polyadenylated (poly(A)⁺) RNA enrichment was performed as described³⁹. Poly(A)⁺ RNA-seq libraries were prepared using Illumina TruSeq Stranded mRNA Sample Prep Kits and subjected to deep sequencing with Illumina NextSeq 500 at the CAS-MPG Partner Institute for Computational Biology Omics Core, CAS. RNA-seq sequencing read quality was evaluated by FastQC (v0.11.5).

Deep sequencing datasets were mapped with TopHat (TopHat v2.0.12, parameters: --microexon-search -g 1 -a 6 -m 2) and aligned to GRCh37/hg19 human reference genome with the UCSC Genes annotation (Human: hg19 knownGene.txt updated at 30 June 2013). Gene expression of linear mRNAs was determined by fragments per kilobase of transcript per million mapped fragments (FPKM). The maximum FPKM of expressed transcript was selected to represent the expression level of each given gene. Refseq genes with FPKM ≥ 1 at least in 1 sample were selected for comparison (Human hg19 refFlat.txt updated at 9 April 2017), and the mean of 2 replicates was calculated as the gene expression level. FC between gRNA (or shRNA) knockdown and RfxCas13d NT (or shRNA NT) was used to determine upregulated (FC ≥ 1.5), unchanged (0.667 $<$ FC $<$ 1.5) and downregulated (FC ≤ 0.667) genes.

Gene Ontology of differentially expressed genes. DEGs after *circFAM120A* knockdown by RfxCas13d-gRNA were identified for GO. Ninety-seven DEGs were manually clustered with GeneCards (<https://www.genecards.org/>) and PubMed (<https://www.ncbi.nlm.nih.gov/pubmed/>). Annotated GO terms (<http://amigo.geneontology.org/amigo>) were employed to classify *circFAM120A*-affected genes on the basis of their functions with a manual check⁴⁰.

Conservation of circRNA analyses. Conservation of the circRNA analysis pipeline was applied as previously reported¹¹, with slight modification. In brief, sequences of back-spliced exons were extracted and used LiftOver tool (<http://genome.ucsc.edu/cgi-bin/hgLiftOver>, parameters: -bedPlus D 3 -tab -minMatch D 0.1 -minBlocks D 1) to identify orthologous coordinates between human (genome version: hg19) and mouse (genome version: mm10). In addition, a human- and mouse-expressed circRNA identified in mouse/human orthologous locus without nucleotide difference in BSJ contexts (± 5 nucleotides) was suggested as a conserved circRNA.

Statistical analyses. Statistically significant differences were assessed using two-tailed Student's *t*-test with the R platform (R v3.5.1). $P < 0.05$, < 0.01 and < 0.001 were marked by 1 asterisk, 2 asterisks or 3 asterisks, respectively. To evaluate the relevant correlation between two datasets, Pearson correlation coefficient and Spearman's rank correlation coefficient were performed with the R platform (R v3.5.1).

Data visualization. Plots were generated with R platform (R v3.5.1) by using ggplot2 (v3.3.0), ggrepel (v0.8.1), corrplot (v0.84), pheatmap (v1.0.12), RColorBrewer (v1.1-2), ggpubr (v0.4.0), magrittr (v1.5) and ggbeeswarm (v 0.6.0) packages. Boxplots were shown as median and interquartile range (IQR). Histograms and line charts were plotted with GraphPad Prism 8 (v8.2.1).

Reporting Summary. Further information on research design is available in the Nature Research Reporting Summary linked to this article.

Data availability

All sequencing datasets have been deposited in NCBI GEO ([GSE149690](https://www.ncbi.nlm.nih.gov/geo/query/acc.cgi?acc=GSE149690), [GSE149691](https://www.ncbi.nlm.nih.gov/geo/query/acc.cgi?acc=GSE149691), and [GSE149692](https://www.ncbi.nlm.nih.gov/geo/query/acc.cgi?acc=GSE149692)) and National Omics Data Encyclopedia ([OEP000887](https://www.ncbi.nlm.nih.gov/omeprj/100087), [OEP000888](https://www.ncbi.nlm.nih.gov/omeprj/1000888) and [OEP000889](https://www.ncbi.nlm.nih.gov/omeprj/1000889)). The total RNA sequences of human H9, FB and PA1 cell lines were downloaded from NCBI GEO ([GSE73325](https://www.ncbi.nlm.nih.gov/geo/query/acc.cgi?acc=GSE73325)). RNA-seq datasets of SH-SY5Y were downloaded from NCBI GEO ([GSE65926](https://www.ncbi.nlm.nih.gov/geo/query/acc.cgi?acc=GSE65926)). RNA-seq datasets of HepG2, K562 cell lines and 11 different human tissues were downloaded from ENCODE Project Consortium (<https://www.encodeproject.org/>). AGO2 PAR-CLIP and miRNA-seq datasets of HEK293 cells were downloaded from NCBI GEO ([GSE43573](https://www.ncbi.nlm.nih.gov/geo/query/acc.cgi?acc=GSE43573) and

[GSE58127](https://www.ncbi.nlm.nih.gov/geo/query/acc.cgi?acc=GSE58127)). IGF2BP2 of eCLIP-seq datasets in K562 cells was downloaded from NCBI GEO ([GSE91445](https://www.ncbi.nlm.nih.gov/geo/query/acc.cgi?acc=GSE91445)). The single-cell RNA-seq transcriptome datasets in mouse preimplantation embryos were from NCBI GEO ([GSE53386](https://www.ncbi.nlm.nih.gov/geo/query/acc.cgi?acc=GSE53386)). Source data are provided with this paper.

Code availability

The custom Perl and Shell scripts for the computational pipeline of Cas13d-mediated circRNA screen (CDCscreen) to identify negatively selected functional circular RNAs in this paper is available at <https://github.com/YangLab/CDCscreen>.

References

37. Yin, Q. F. et al. Long noncoding RNAs with snoRNA ends. *Mol. Cell* **48**, 219–230 (2012).
38. Li, S. et al. Screening for circRNAs with functional potential using the RfxCas13d/gRNA library. *Protocol Exchange* <https://doi.org/10.21203/rs.3.pex-1181/v1> (2020).
39. Yang, L., Duff, M. O., Graveley, B. R., Carmichael, G. G. & Chen, L. L. Genomewide characterization of non-polyadenylated RNAs. *Genome Biol.* **12**, R16 (2011).
40. Wang, Y. et al. Genome-wide screening of NEAT1 regulators reveals cross-regulation between paraspeckles and mitochondria. *Nat. Cell Biol.* **20**, 1145 (2018).
41. Dong, R., Ma, X. K., Li, G. W. & Yang, L. CIRCPedia v2: an updated database for comprehensive circular RNA annotation and expression comparison. *Genomics Proteom. Bioinforma.* **16**, 226–233 (2018).

Acknowledgements

We thank Chen and Yang laboratories for discussion. This work was supported by the Chinese Academy of Sciences (CAS) (XDB19020104), the National Natural Science Foundation of China (NSFC) (91940303, 31821004, 31725009) and the HHMI International Program (55008728) to L.-L.C. NSFC (31730111, 31925011, 91940306) to L.Y.; NSFC (31730062, 31821004) and the Shanghai Municipal Commission for Science and Technology (19411951800) to J.L.; NSFC (31801073) and the Youth Innovation Promotion Association CAS to W. X.

Author contributions

L.-L.C. supervised and conceived the project. L.-L.C., L.Y., J.L., S.L., X.L., W.X. and L.Z. designed experiments. L.Z. performed circRNA screening in mouse embryos, supervised by J.L.; S.L., X.L., L.-Z.Y., S.-M.C., C.-X.L., S.-K.G., L.S., M.W., X.T., J.-L.Z., X.G., J.Z. and J.W. performed all other experiments; W.X., Y.-N.L. and L.Y. performed computational analyses. L.-L.C. and L.Y. wrote the paper with input from S.L., X.L., W.X. and J.L.

Competing interests

The authors declare no competing interests.

Additional information

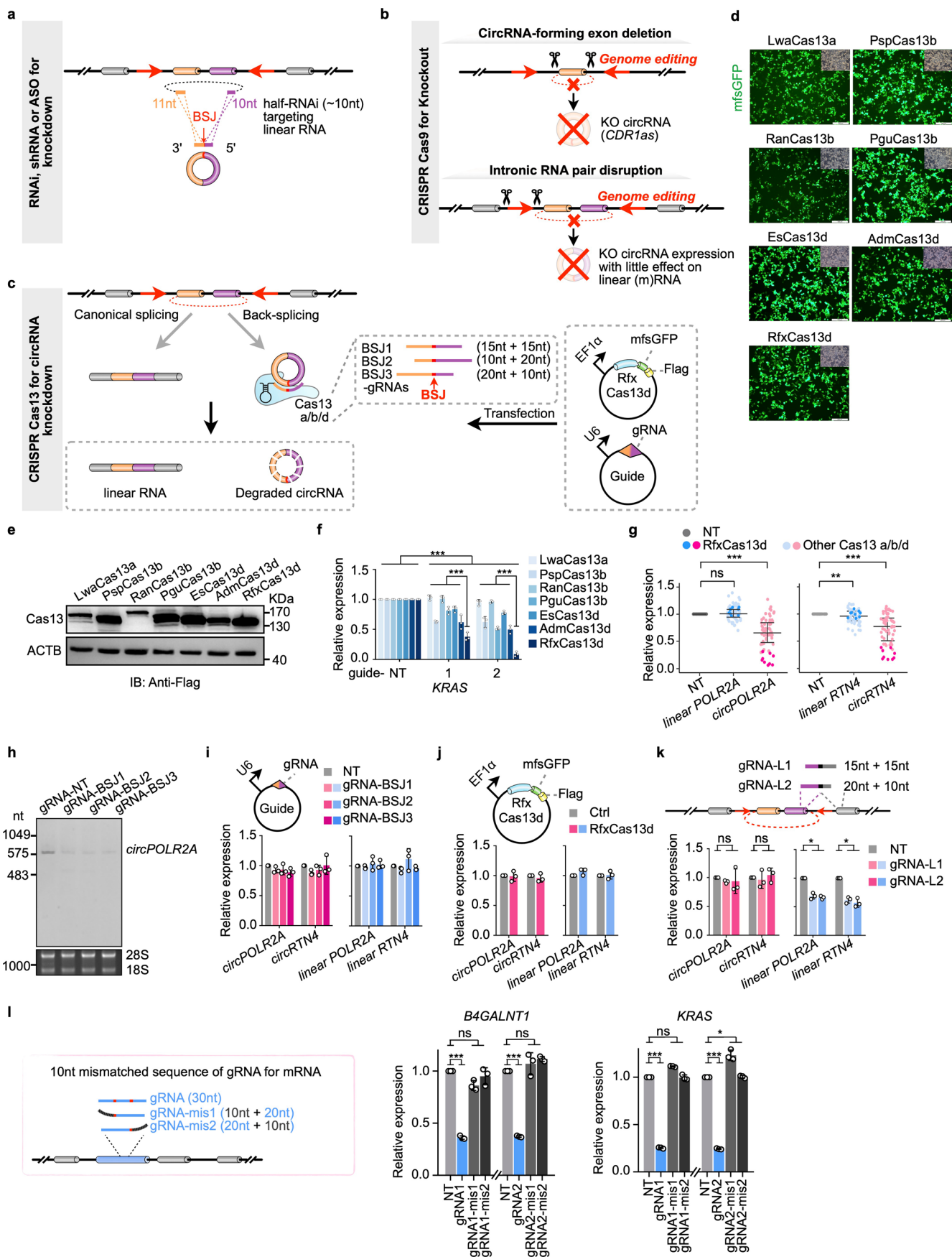
Extended data is available for this paper at <https://doi.org/10.1038/s41592-020-01011-4>.

Supplementary information is available for this paper at <https://doi.org/10.1038/s41592-020-01011-4>.

Correspondence and requests for materials should be addressed to J.L., L.Y. or L.-L.C.

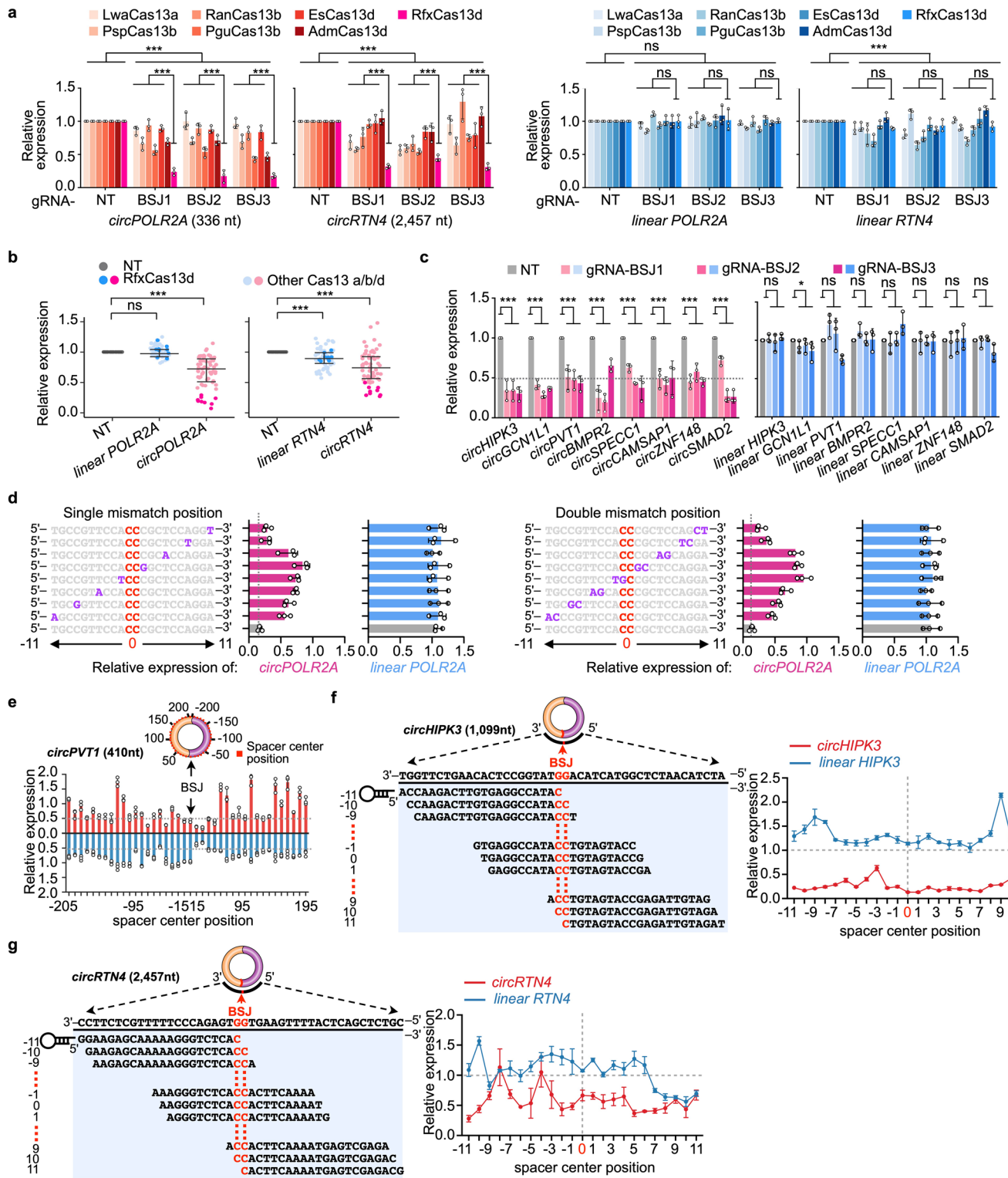
Peer review information *Nature Methods* thanks the anonymous reviewers for their contribution to the peer review of this work. Lei Tang was the primary editor on this article and managed its editorial process and peer review in collaboration with the rest of the editorial team.

Reprints and permissions information is available at www.nature.com/reprints.



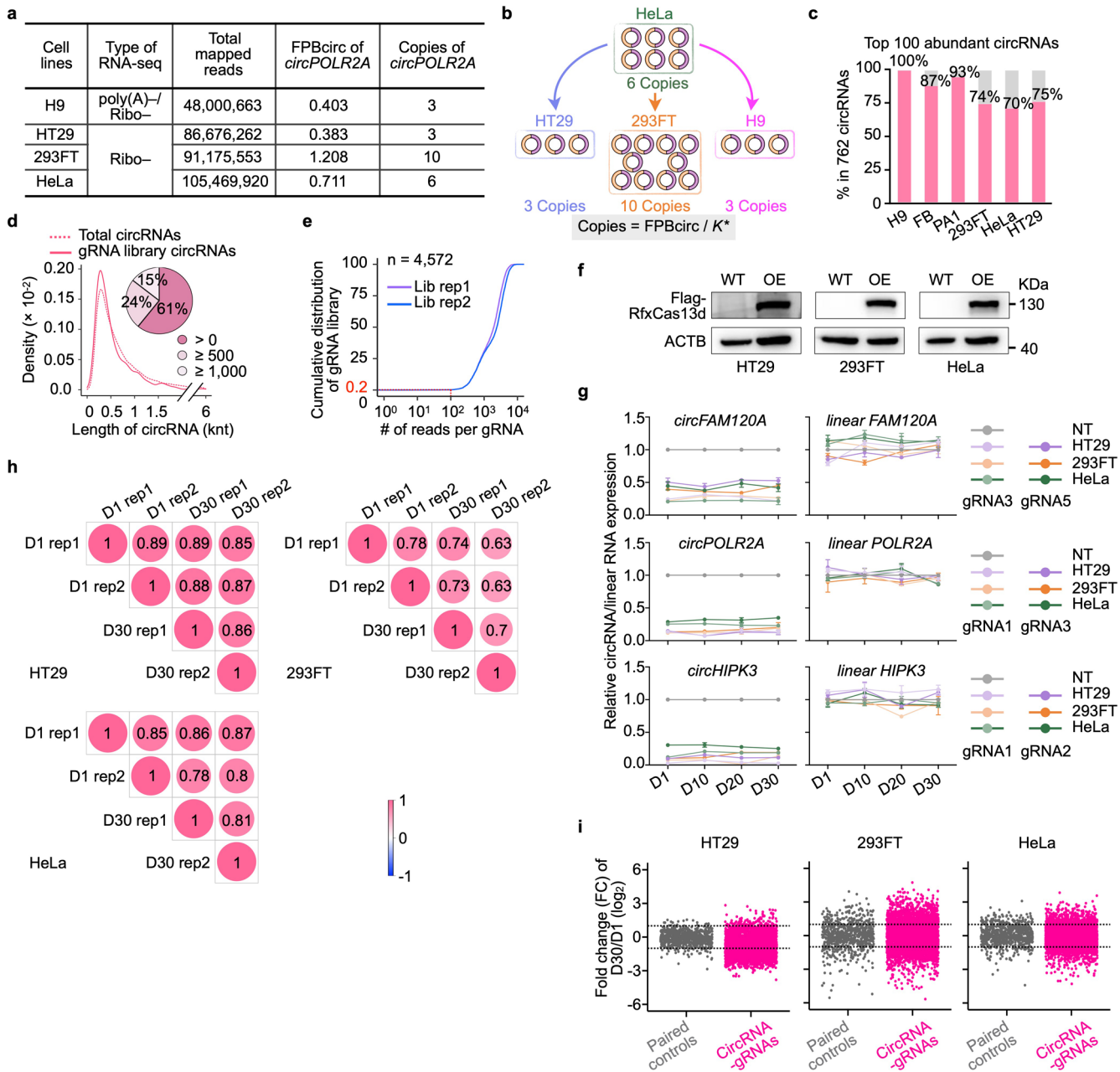
Extended Data Fig. 1 | See next page for caption.

Extended Data Fig. 1 | Evaluation of RfxCas13d knockdown efficiency and specificity. **a**, Strategies of circRNA knockdown (KD) by RNAi, shRNA and ASO. **b**, Strategies of circRNA knockout by CRISPR/Cas9. Top, genome editing is used to remove circRNA-formed exons⁵; bottom, genome editing destroys the intronic RNA pair to block circRNA expression^{6,7}. **c**, Schematic of circRNA KD by Cas13. Three gRNAs targeting the back-splicing junction site (BSJ, red arrow) were designed for each circRNA (BSJ-gRNAs). Expression of circRNAs and cognate linear mRNAs were detected by qRT-PCR. **d,e**, Expression of Cas13 proteins were detected by msfGFP fluorescence (**d**) and WB (**e**) in 293FT cells after 48 h transfection. Scale bar, 200 μ m. Results are representative of two independent experiments. **f**, Comparison of different Cas13 proteins-mediated KRAS knockdown efficiencies with two position-matched guides revealed that RfxCas13d is the best effector¹⁴. **g**, Evaluation of different Cas13-protein-mediated KD on circRNAs. $n = 63$ biologically independent samples. Data are presented as means values \pm s.d. **h**, NB confirmed the *circPOLR2A* knockdown by RfxCas13d/BSJ-gRNAs. Results are representative of two independent experiments. **i,j**, BSJ gRNAs (**i**) or RfxCas13d (**j**) alone did not affect *circPOLR2A* and *circRTN4* expression. **k**, gRNAs with partial sequences replaced by adjacent linear exon (gRNA-L) led to linear but not circular RNA KD. Top, schematic of gRNA-L. Bottom, KD efficiencies of *circPOLR2A* and *circRTN4* as well as their corresponding linear RNAs. **l**, Replacement of a 10nt (scram/mismatch) on either side of an originally highly effective 30nt gRNA (blue bars) completely blocked the KD effect on the target mRNAs. Two 30nt effective gRNAs and the corresponding 10(scram/mismatch) + 20nt gRNAs on two individual mRNAs were tested. (**f,i,j,k,l**) All expression levels of RNAs were detected by qRT-PCR and were normalized to *ACTB*, means \pm s.d. were from three independent experiments. (**f,g,j,k,l**) *: $P < 0.05$; **: $P < 0.01$; ***: $P < 0.001$; ns, not significant, two-tailed student's *t*-test.



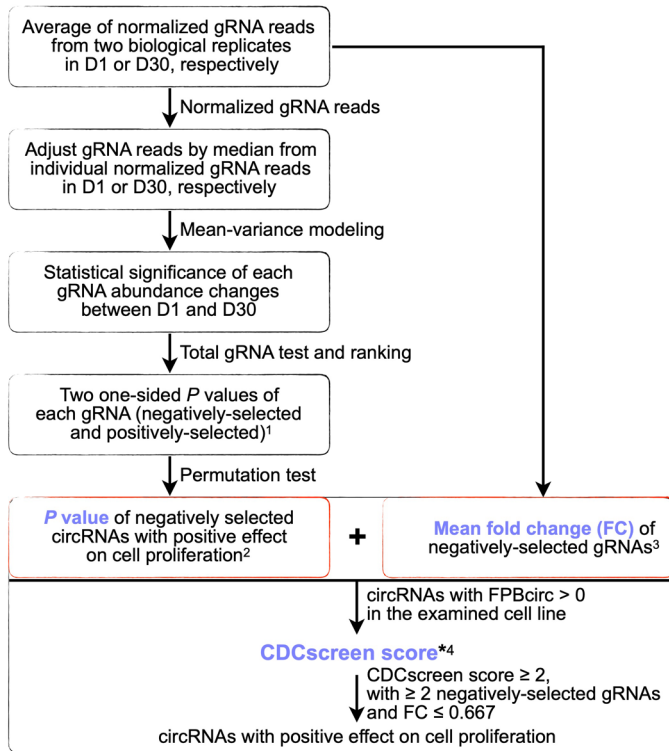
Extended Data Fig. 2 | See next page for caption.

Extended Data Fig. 2 | RfxCas13d is the best effector to mediate circRNA knockdown. **a,b**, Evaluation of Cas13 proteins for knocking down circRNAs (*circPOLR2A* and *circRTN4*) and their cognate mRNAs in HeLa cells revealed that RfxCas13d is the best effector for circRNA-specific KD. **b**, $n=63$ biologically independent samples and transcript levels were normalized to ACTB. Data are presented as means values \pm s.d. **c**, RfxCas13d/BSJ-gRNAs specifically and robustly knocked down circRNAs, but not their cognate mRNAs in HeLa cells. **d**, Mismatch tolerance of RfxCas13d for circRNA targeting. Guides containing single or double mismatches at varying positions across spacer sequences for *circPOLR2A* are shown in purple; bases flanking the BSJ site are shown in red. **e**, Efficiency and specificity of RfxCas13d for circRNA and cognate linear mRNA KD. Top, schematic of gRNAs targeting *circPVT1* tiled 10-nt increments away from the BSJ site. Bottom, KD efficiencies of circRNA and linear RNA by each gRNA and RfxCas13d. **f-g**, Arrayed KD screen of 23 guides evenly tiled across BSJ of *circHIPK3* (**f**) and *circRTN4* (**g**). Position-effect of BSJ-gRNAs for RfxCas13d-mediated KD of *circHIPK3* (**f**) and *circRTN4* (**g**) at the single nucleotide level. Twenty-three guides tiled across the BSJ of *circHIPK3* (**f**) and *circRTN4* (**g**) are listed. KD efficiencies of *circHIPK3* (**f**) or *circRTN4* (**g**) and linear *HIPK3* (**f**) or linear *RTN4* (**g**) by each BSJ-gRNA were shown in the right. **(a,c,d,e,f,g)** All expression levels of RNAs were detected by qRT-PCR and were normalized to *ACTB*, means \pm s.d. were from three independent experiments. **(a,b,c)** **: $P < 0.01$; ***: $P < 0.001$; ns, not significant, two-tailed student's *t*-test.

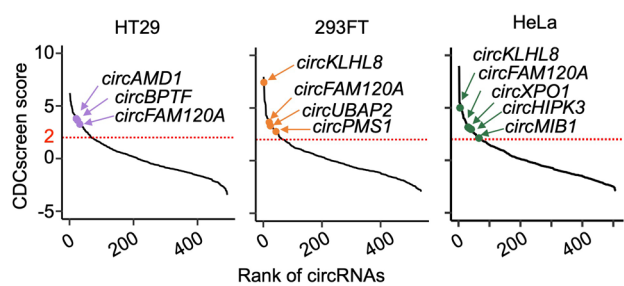


Extended Data Fig. 3 | Characterization of the BSJ-gRNA library targeting 762 circRNAs. **a**, Calculation of circRNA copy numbers (using *circPOLR2A* as an example) in H9, HT29, HeLa and 293FT cells. According to the FPCirc of *circPOLR2A* and other circRNAs in H9, HT29, HeLa and 293FT cells, and the six copies of *circPOLR2A* per HeLa cell¹⁷, we calculated the copy number of all circRNAs, respectively. Copies of *circPOLR2A* per cell were listed. **b**, Schematic of circRNA copy number calculation in H9, HT29, HeLa and 293FT cells. **c**, Representation of 762 candidate circRNAs designed with BSJ-gRNAs in the library in different cell lines. **d**, Matched length distribution of 762 candidate circRNAs (solid line) and total circRNAs (dashed line). Density curve and pie chart show that more than 80% of 762 candidate circRNAs and total circRNAs are less than 1,000nt. **e**, Cumulative distribution of the number of reads per gRNA of constructed libraries. The red line indicates that less than 0.2% of gRNAs are covered by less than 100 reads. **f**, WB confirmed the stable expression of Flag-RfxCas13d in HT29, 293FT and HeLa cells used for screening. Results are representative of two independent experiments. **g**, KD efficiency of circRNAs remained unchanged in 30 days. RfxCas13d/BSJ-gRNA infected HT29, 293FT and HeLa cells were collected at a series of timepoints (day 1, 10, 20, 30). KD efficiency of different circRNAs was detected by qRT-PCR and were normalized to ACTB. Means \pm s.d. were from three independent experiments. **h**, Pearson correlation coefficient (PCC) between replicates (rep) of D1 and D30 samples in HT29, 293FT and HeLa cells. Two biologically independent experiments were performed at D1 and D30 in each cell line. **i**, Scatter plot of fold change of paired controls and circRNA BSJ-gRNAs between D1 and D30 samples in HT29, 293FT and HeLa cells. The grey dashed lines indicate 2 or 0.5 fold change, respectively.

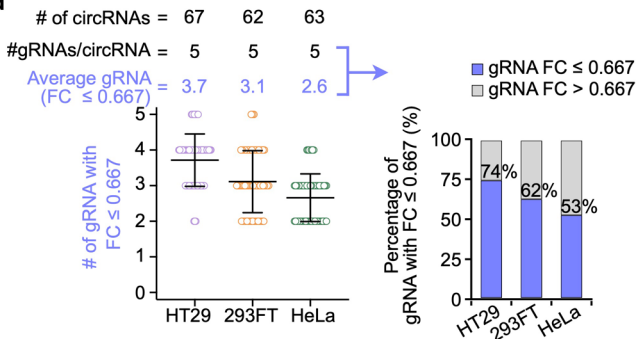
a

CDCscreen

b



d

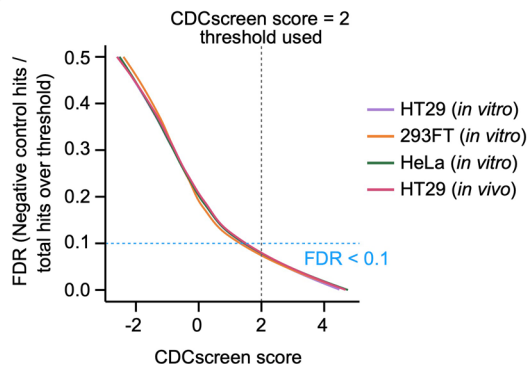


c

| CircRNA in HT29 (<i>in vitro</i>) | CircRNA host gene symbol | gRNA ID | ¹ One-sided P values of gRNA | ² P value of circRNA | ³ Mean FC of negatively-selected gRNAs | Expression of circRNA (FPBcirc) | ⁴ CDCscreen score | FDR | Fold change of negatively-selected gRNAs |
|-------------------------------------|--------------------------|---------|---|---------------------------------|---|---------------------------------|------------------------------|---------|--|
| chr9:96233422-96261168 | <i>FAM120A</i> | gRNA1 | 0.33427 | 0.047407 | 0.374875 | 1.78198 | 3.26981 | 0.02333 | 0.6 |
| | | gRNA2 | 0.53627 | | | | | | 1.5 |
| | | gRNA3 | 0.11439 | | | | | | 0.3 |
| | | gRNA4 | 0.10973 | | | | | | 0.2 |
| | | gRNA5 | 0.268 | | | | | | 0.4 |

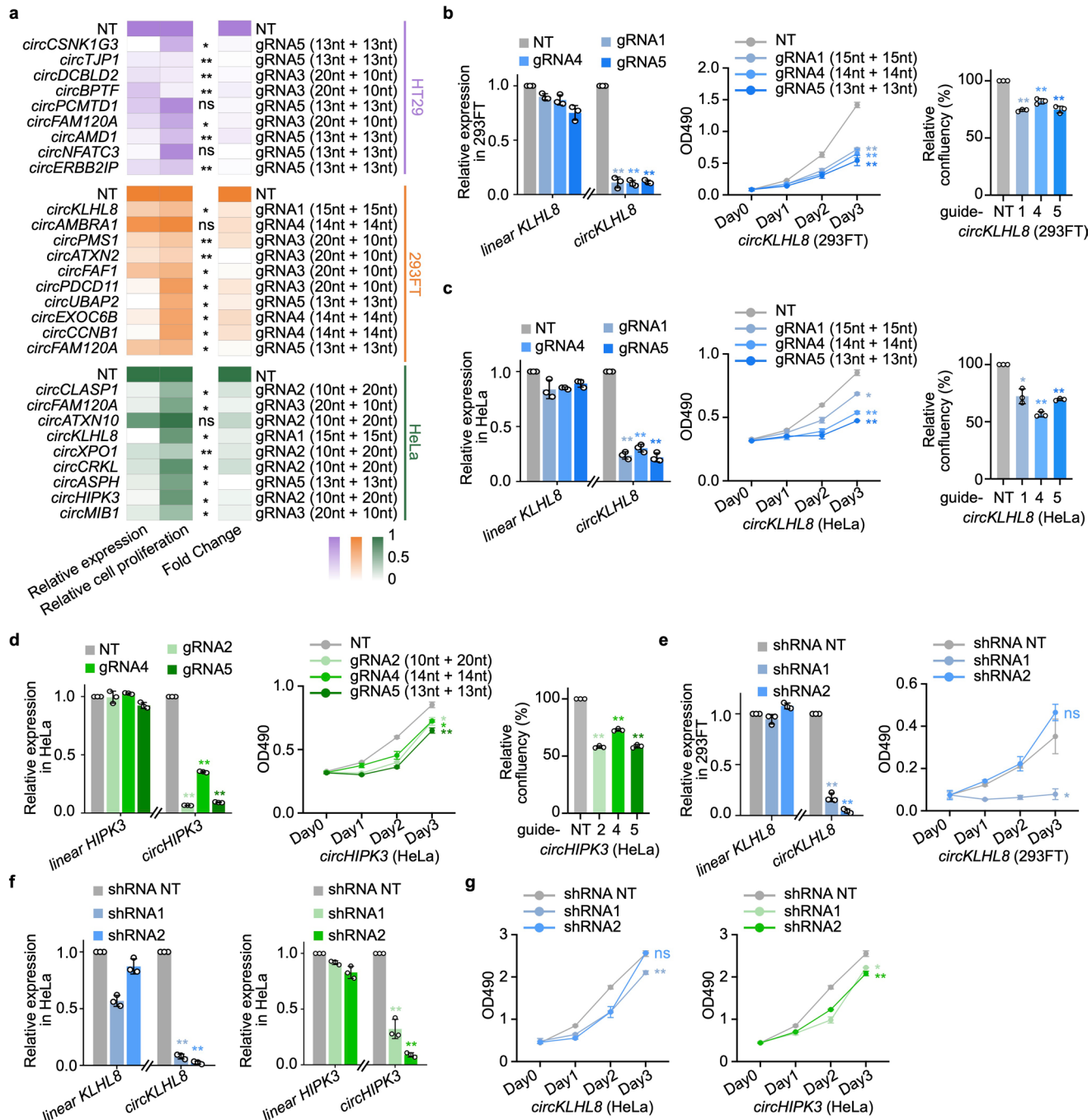
1,2,3,4 were correspond to Fig. a in this Figure

e

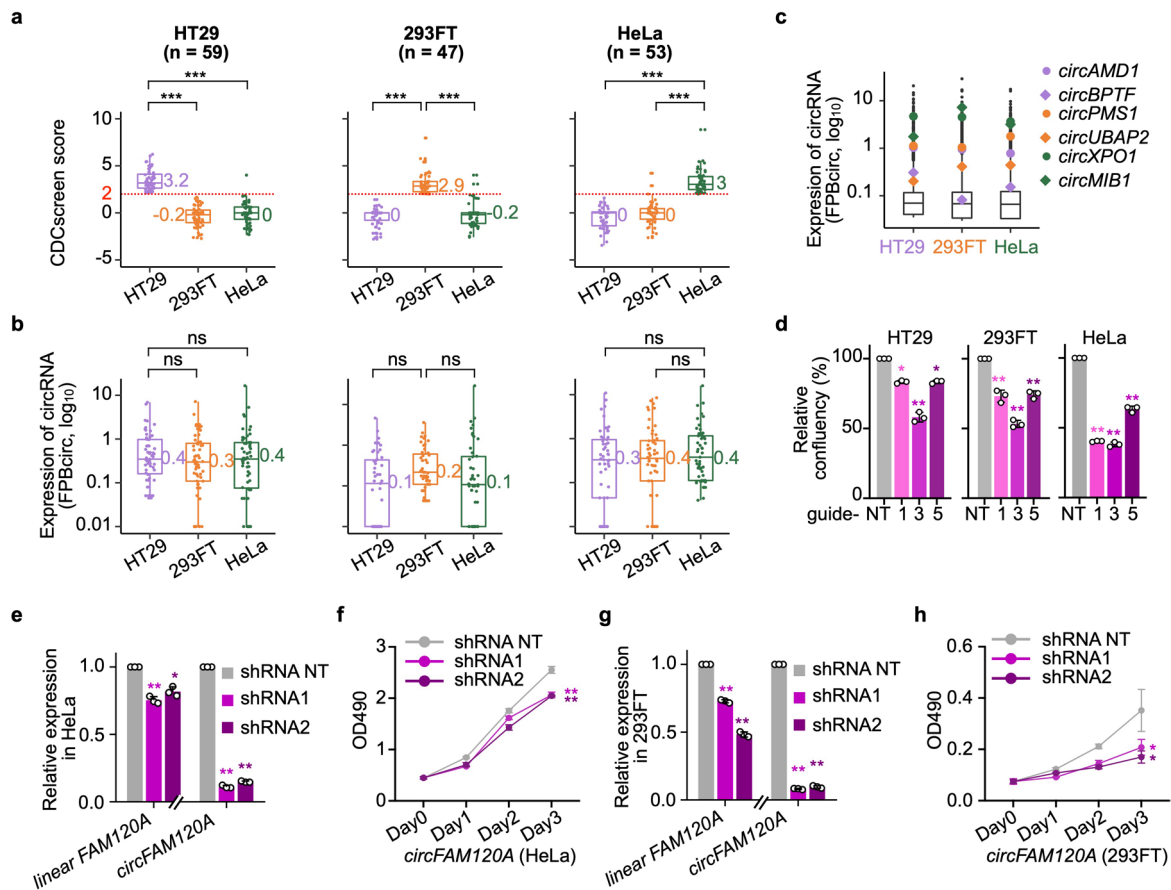


Extended Data Fig. 4 | See next page for caption.

Extended Data Fig. 4 | Pipelines used to identify negatively selected candidate circRNAs important for cell growth. **a**, Analysis pipeline to identify negatively selected circRNA candidates by CDCscreen. Uniquely-mapped reads of each gRNA were normalized, and averaged normalized reads of two biological replicates were used for subsequent analyses. P value of negatively selected circRNA was computed by the permutation test of MAGeCK, and mean fold change of negatively-selected gRNAs targeting the same circRNAs between D30 and D1 treatments was obtained from normalized gRNA reads. Only expressed circRNAs with $\text{FPBcirc} > 0$ were calculated. Finally, circRNAs with CDCscreen score ≥ 2 , ≥ 2 negatively-selected gRNAs with $\text{FC} \leq 0.667$ were identified as circRNA candidates to promote cell proliferation. **b**, Rank of negatively selected candidate circRNAs by CDCscreen scores in HT29, 293FT and HeLa cells. CircRNAs with CDCscreen score ≥ 2 and with ≥ 2 negatively-selected gRNAs and $\text{FC} \leq 0.667$ were sub-grouped by red dashed line. Examples of candidate circRNAs were marked in each cell line. **c**, Each item in the table corresponds to each step of calculation of candidate circRNAs in CDCscreen pipeline shown in **(a)**. *CircFAM120A* is shown as an example, and related analyses of all other circRNAs are listed in Supplementary Table 4. **d**, Analysis of gRNAs in $\text{FC} \leq 0.667$ that identifies the same circRNA as a target gene. The number of circRNA candidates, the average total gRNAs and altered gRNAs in $\text{FC} \leq 0.667$ (purple) in each cell line are shown. $n = 67$ circRNAs in HT29, $n = 62$ circRNAs in 293FT, $n = 63$ circRNAs in HeLa. Data are presented as means values \pm s.d. **e**, False discovery rate (FDR) of circRNA candidates with CDCscreen score ≥ 2 is less than 0.1 for *in vitro* (Fig. 2b) and *in vivo* (Extended Data Fig. 7a) screens.

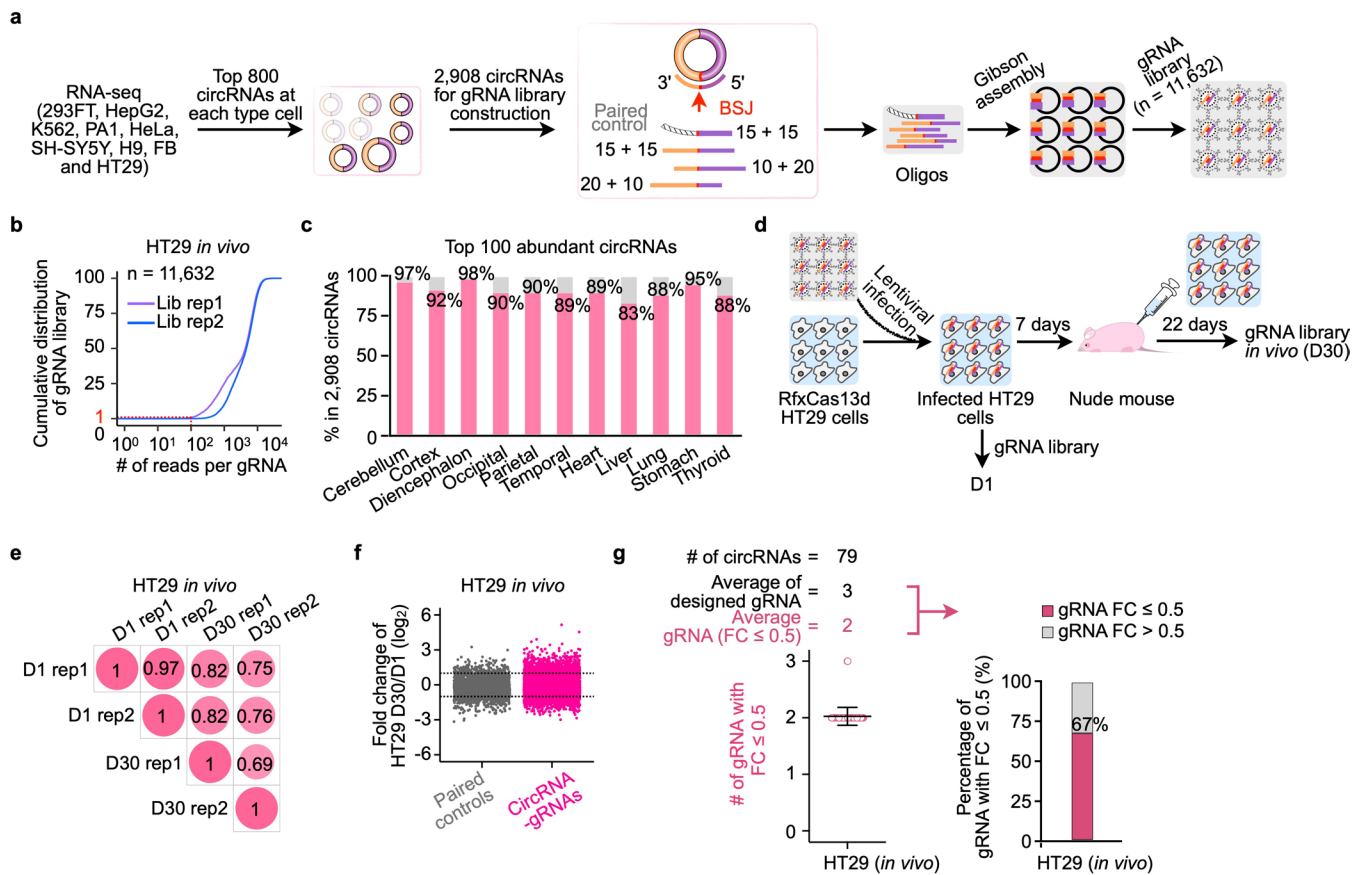


Extended Data Fig. 5 | Validation of candidate circRNAs by the RfxCas13d/BSJ-gRNA system in cell proliferation. **a**, Heatmap display of the relative KD efficiency, cell proliferation and fold change of candidate circRNAs in HT29 (purple), 293FT (orange) and HeLa (green) cells with single BSJ-gRNA that targets each candidate circRNA. **b,c**, KD of *circKLHL8* by RfxCas13d inhibited cell proliferation in 293FT (**b**) and HeLa cells (**c**), as revealed by MTT cell proliferation assay (middle panels) and cell confluency calculated by the surface area occupied by cells (right panels); KD efficiencies were showed on left panels. **d**, KD of *circHIPK3* by RfxCas13d inhibited cell proliferation in HeLa cells, as revealed by MTT cell proliferation assay (middle) and by cell confluency calculated by the surface area occupied by cells (right); KD efficiencies were showed on left. **e**, KD of *circKLHL8* by shRNAs inhibited cell proliferation in 293FT cells. KD efficiencies were showed on left; MTT cell proliferation assays were shown on right. **f**, KD of *circKLHL8* and *circHIPK3* by shRNAs in HeLa cells. **g**, KD of *circKLHL8* or *circHIPK3* by shRNAs inhibited cell proliferation in HeLa cells, as revealed by MTT cell proliferation assays. (**a,b,c,d,e,f**) All expression levels of RNAs were detected by qRT-PCR and were normalized to ACTB. Means \pm s.d. were from three independent experiments. * $P < 0.05$; ** $P < 0.01$; ns, not significant, two-tailed student's t-test.

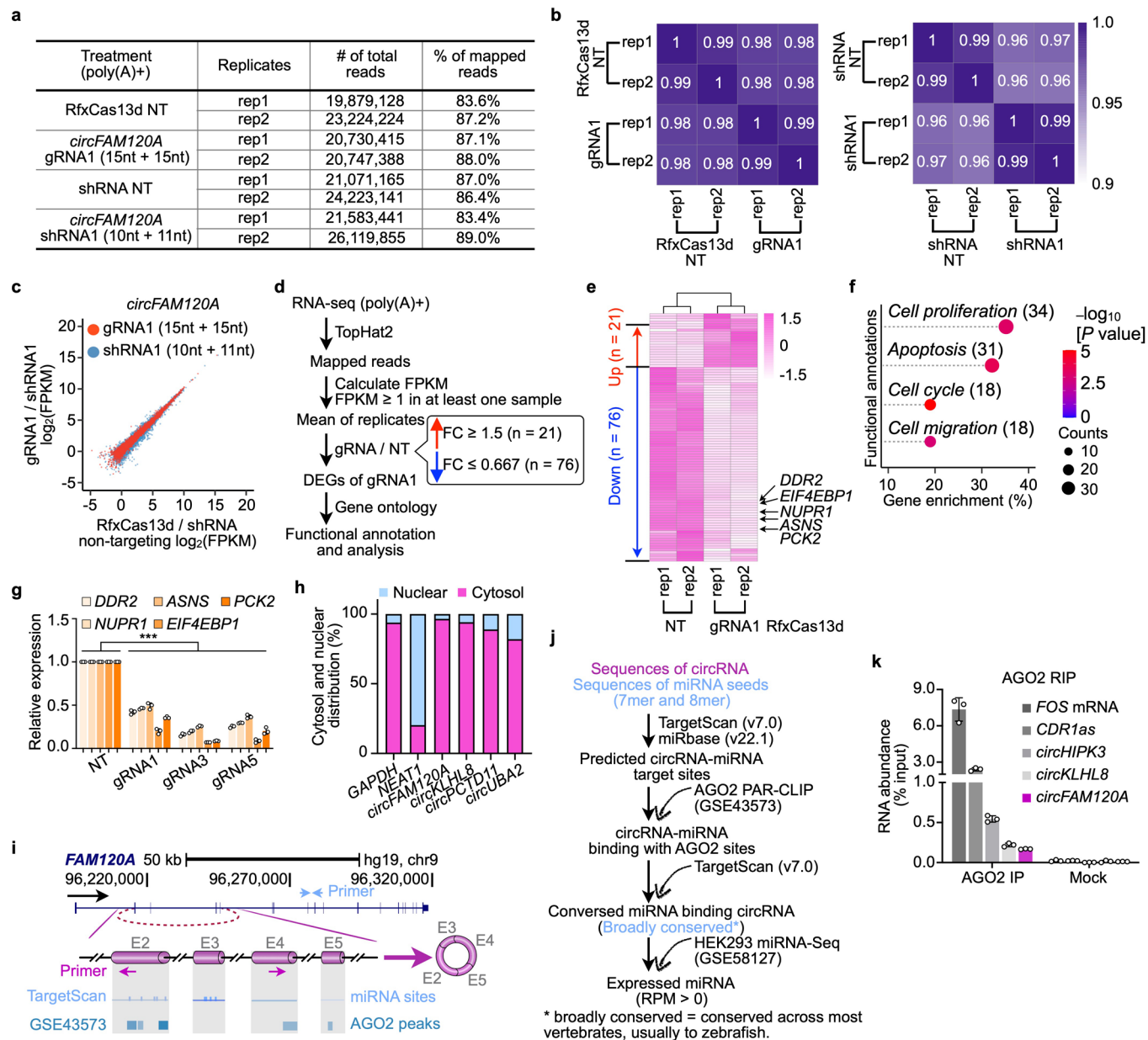


Extended Data Fig. 6 | Distribution of CDCscreen scores and expression levels of circRNAs that have cell type-specific effects on cell growth.

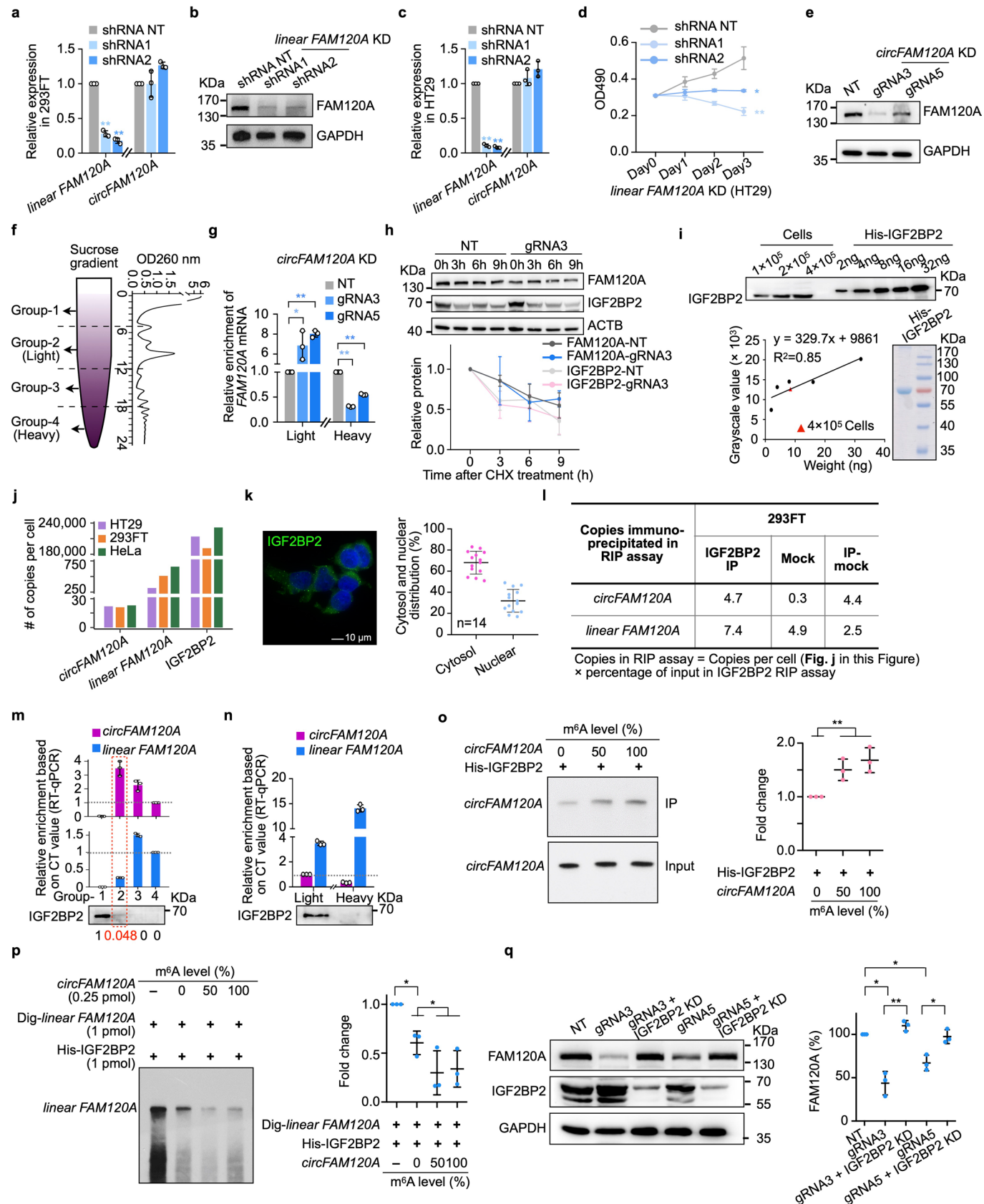
a, Distribution of CDCscreen scores of circRNAs with cell-type specific effects on cell proliferation in HT29 (n=59 circRNAs), 293FT (n=47 circRNAs) and HeLa (n=53 circRNAs) cell, respectively. See ‘Data visualization’ in the Methods for definitions of box plot elements. **b**, Expression (shown by FPBcirc, log₁₀) of circRNAs shown in **(a)** in HT29 (n=59 circRNAs), 293FT (n=47 circRNAs) and HeLa (n=53 circRNAs) cells. See ‘Data visualization’ in the Methods for definitions of box plot elements. **c**, Expression (shown by FPBcirc, log₁₀) of validated circRNAs (n=6) in Fig. 2d that have cell-type specific effects on cell proliferation in HT29, 293FT and HeLa cells. See ‘Data visualization’ in the Methods for definitions of box plot elements. **d**, CircFAM120A KD by RfxCas13d/BSJ-gRNAs inhibited HT29, 293FT or HeLa cell proliferation, as revealed by cell confluence assays. **e**, CircFAM120A KD by shRNAs in HeLa cells. Expression of circRNAs and cognate linear RNAs was detected by qRT-PCR and was normalized to ACTB. **f**, CircFAM120A KD by shRNAs inhibited cell proliferation in HeLa cells, as revealed by MTT assays. **g**, CircFAM120A KD by shRNAs in 293FT cells. Expression of circRNAs and cognate linear RNAs was detected by qRT-PCR and was normalized to ACTB. **h**, CircFAM120A KD by shRNAs inhibited cell proliferation in 293FT cells, as revealed by MTT assays. (**d,e,f,g,h**) Means \pm s.d. were from three independent experiments. (**a,b,d,e,f,g,h**) *: P < 0.05; **: P < 0.01; ***: P < 0.001; ns, not significant, two-tailed student’s t-test.



Extended Data Fig. 7 | Overview of sequencing analyses of *in vivo* screens using BSJ-gRNA libraries targeting 2,908 circRNAs. **a**, Construction of the gRNA library targeting 2,908 circRNAs. One paired control gRNA ($n=2,908$) and three BSJ-gRNAs (circRNA gRNAs, $n=8,724$) were designed for each candidate circRNA. **b**, Cumulative distribution of the number of reads per gRNA of constructed libraries. The red line indicates that less than 1% of gRNAs are covered by less than 100 reads. **c**, Representation of 2,908 candidate circRNAs in different human tissues⁴¹ constructed in the library. On average, over 90% of top 100 abundant circRNAs in each tissue were included in the list of 2,908 candidate circRNAs. **d**, *In vivo* screen of circRNAs important for cell growth and proliferation. The gRNA lentiviral library was individually delivered into HT29 cells stably expressing RfxCas13d. Infected cells were enriched after 7 days and injected subcutaneously to nude mouse for 22 days. Genomic DNAs from infected cells were extracted at day 1 (D1) and 30 (D30) for gRNA amplification and deep sequencing. **e**, The Pearson correlation coefficient (PCC) between replicates (rep) of D1 and D30 *in vivo* samples in HT29. Two biologically independent experiments were performed at D1 and D30. **f**, Scatter plot of fold change of paired controls and circRNA BSJ-gRNAs between D1 and D30 *in vivo* samples in HT29. The grey dashed lines indicate 2 or 0.5 fold change, respectively. **g**, Analysis of gRNAs in $FC \leq 0.5$ that identifies the same circRNA as a target gene. The number of circRNA candidates ($n=79$), the average total gRNAs and altered gRNAs in $FC \leq 0.5$ (purple) in *in vivo* screen are shown. Data are presented as means values \pm s.d.



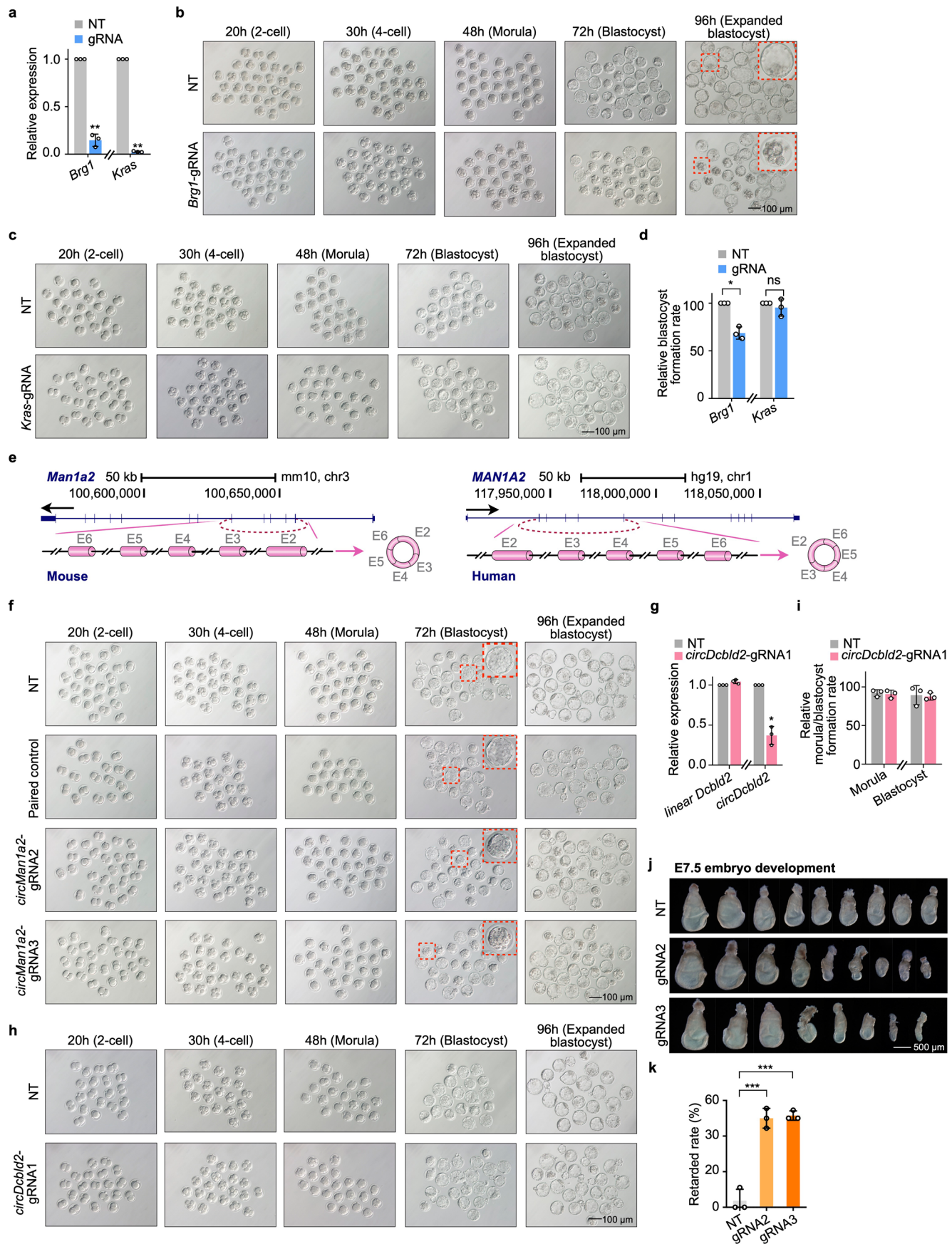
Extended Data Fig. 8 | RNA-seq analysis of RfxCas13d/BSJ-gRNA- or shRNA- mediated *circFAM120A* KD. **a**, Mapping statistics of two biological replicates of the poly(A)+ RNA-seq datasets in 293FT cells with RfxCas13d/BSJ-gRNA- or shRNA- mediated *circFAM120A* KD. **b**, Heatmap of Spearman's rank correlation coefficient for $\log_2(\text{FPKM})$ values of all linear mRNAs detected in RNA-seq libraries between targeting and non-targeting replicates for RfxCas13d/BSJ-gRNA- or shRNA- mediated *circFAM120A* KD. **c**, Expression levels in $\log_2(\text{FPKM})$ values of all genes detected in RNA-seq libraries of non-targeting control (x-axis) compared to *circFAM120A*-targeting conditions (y-axis) by RfxCas13d/BSJ-gRNA (red) or shRNA (blue). Means of two biological replicates were shown. **d**, A workflow shows the selection of candidate genes after *circFAM120A* KD by RfxCas13d/BSJ-gRNA. **e**, Heatmap of DEGs (n=97) detected after *circFAM120A* KD by RfxCas13d/BSJ-gRNA. **f**, Enrichment of DEGs from RNA-seq after *circFAM120A* KD by RfxCas13d/BSJ-gRNA. The x axis shows the ratio of the number of genes in a given category of functional annotations divided by the total number of DEGs. The y axis shows categories of functional annotations. *P* values were calculated based on the Fisher's exact test. **g**, Validation of DEGs associated with cell proliferation after *circFAM120A* KD by RfxCas13d/BSJ-gRNA in 293FT cells. All transcripts were normalized to ACTB, n=3 independent experiments. ***: $P < 0.001$, two-tailed student's *t*-test. **h**, Cytoplasmic distribution of *circFAM120A*. **i**, Prediction of AGO2-binding peaks in *circFAM120A*. Top, genomics locus and diagram of linear *FAM120A* and *circFAM120A* (shown as magenta cylinders). Blue and magenta arrows indicate location of primer for linear *FAM120A* or *circFAM120A*. Bottom, predicted miRNA target sites by TargetScan and AGO2 binding peaks from PAR-CLIP data in HEK293FT cells (GEO: GSE43573). **j**, A schematic to show predication of potential circRNA-miRNA target sites. **k**, *CircFAM120A* did not interact with AGO2 by RIP in 293FT cells using anti-AGO2 antibodies. (g,h,k) All RNA levels were detected by qRT-PCR and means \pm s.d. were from three independent experiments.



Extended Data Fig. 9 | See next page for caption.

Extended Data Fig. 9 | CircFAM120A promotes cell proliferation by regulating its parental gene translation in an IGF2BP2-dependent manner.

a,c, KD of FAM120A mRNA by shRNAs in 293FT (**a**) and HT29 (**c**) cells. **b**, Stable KD FAM120A by two shRNAs in 293FT cells, confirmed by one WB experiment. **d**, KD of FAM120A mRNA by shRNAs inhibited cell proliferation in HT29 cells, revealed by MTT assays. **e**, *circFAM120A* KD by two gRNAs reduced FAM120A protein expression in HT29 cells, confirmed by WB of one experiment; see also three independent experiments in 293FT cells (Fig. 3c). **f**, Schematic of sucrose gradients used to segregate fractions in polysome profiling assays. The light fraction contains ribosome subunits and single ribosomes; the heavy fraction contains polyribosomes. **g**, *CircFAM120A* KD led to altered distribution of FAM120A mRNA on ribosomes. FAM120A mRNA in individual fractions were measured by qRT-PCR and were normalized to GAPDH. **h**, Stability of FAM120A protein remains unchanged after *circFAM120A* KD. Cycloheximide (CHX) was used to inhibit translation. Quantification of results from duplicated assays was shown underneath. **i**, Absolute quantification of IGF2BP2 copies per cell. Results are representative of three experiments. **j**, Copies of *circFAM120A*, linear FAM120A and IGF2BP2 protein per HT29, 293FT or HeLa cells. **k**, IGF2BP2 was mainly localized in the cytoplasm. Left, representative image of IGF2BP2 immunofluorescence. Right, statistics of IGF2BP2 signals in each image. n=14 images. Data are presented as means values \pm s.d. **l**, Absolute copies of *circFAM120A* and linear FAM120A associated with IGF2BP2, calculated from IGF2BP2 RIP assays in 293FT cells (Fig. 3g). **m-n**, Distribution of IGF2BP2 protein, *circFAM120A* and FAM120A mRNA in fractions of polysome profiling of 293FT cells. **o**, m⁶A promoted *circFAM120A* binding to IGF2BP2 *in vitro*, detected by NB. **p**, m⁶A enhanced the capability of *circFAM120A* to compete with linear FAM120A binding to IGF2BP2 *in vitro*. Dig-labeled linear FAM120A associated with His-IGF2BP2 was detected by NB. **q**, Expression of FAM120A protein was partially rescued by loss of IGF2BP2 in *circFAM120A* KD 293FT cells, revealed by WB. (**a,c,d,g,h,m,n,o,p,q**) Means \pm s.d. are from three independent experiments. (**a,c,d,g,o,p,q**) *: P < 0.05; **: P < 0.01, two-tailed student's t-test. (**h, o, p, q**) Statistics were quantified from three independent experiments processed in parallel.



Extended Data Fig. 10 | See next page for caption.

Extended Data Fig. 10 | Application of RfxCas13d/gRNA to interfere RNA expression during mouse preimplantation development. **a**, KD of *Brg1* and *Kras* by RfxCas13d/gRNA in zygotes. Expression of mRNAs was detected by qRT-PCR and normalized to *Actb*. **b**, Representative images of reduced blastocyst formation 96 h after microinjection of RfxCas13d mRNA and the gRNA targeting *Brg1* mRNA into mouse zygotes. An example of failed blastocyst formation is shown by red arrows and enlarged view. **c**, Representative images of embryogenesis after microinjection of RfxCas13d mRNA and the gRNA targeting *Kras* mRNA into mouse zygotes. No aberrant mouse preimplantation development was observed. **d**, Effect of *Brg1* (**b**) and *Kras* (**c**) KD on blastocyst formation 96 h after microinjection of RfxCas13d mRNA and BSJ-gRNAs into mouse zygotes. **e**, Diagrams of mouse *circMan1a2* and human *circMAN1A2* are shown as magenta cylinders. **f**, KD of *circMan1a2* in zygotes led to reduced blastocyst formation 72 h after microinjection of RfxCas13d mRNA and BSJ-gRNAs into mouse zygotes. Representative images of at 2-cell, 4-cell, morula and blastocyst stages are shown; an example under each condition is highlighted by red line and enlarged view. **g**, KD of *circDcbld2* by RfxCas13d/BSJ-gRNA in zygotes. Expression of *circDcbld2* was detected by qRT-PCR and normalized to *Actb*. **h**, Images of normal embryonic morphologies at 2-cell, 4-cell, morula and blastocyst stages under *circDcbld2* KD by RfxCas13d/BSJ-gRNA in zygotes. **i**, Statistics of *circDcbld2* KD effectd on morula and blastocyst formation after microinjection of RfxCas13d mRNA and BSJ-gRNAs into mouse zygotes. **j,k**, Implantation of RfxCas13d-gRNA (*circMan1a2* KD)-injected zygotes to pseudo-pregnant female mice led to retarded mouse postimplantation development in E7.5. Images of E7.5 embryos shown in (**j**); statistics of retarded embryos shown in (**k**). **(a,d,g,h,i,j,k)** Means \pm s.d. are from three independent experiments. **(b,c,f,h,j)** Results are representative of three independent experiments. **(a,d,g,k)** *: $P < 0.05$; **: $P < 0.01$; ***: $P < 0.001$; ns, not significant, two-tailed student's *t*-test.

Reporting Summary

Nature Research wishes to improve the reproducibility of the work that we publish. This form provides structure for consistency and transparency in reporting. For further information on Nature Research policies, see our [Editorial Policies](#) and the [Editorial Policy Checklist](#).

Statistics

For all statistical analyses, confirm that the following items are present in the figure legend, table legend, main text, or Methods section.

n/a Confirmed

- The exact sample size (n) for each experimental group/condition, given as a discrete number and unit of measurement
- A statement on whether measurements were taken from distinct samples or whether the same sample was measured repeatedly
- The statistical test(s) used AND whether they are one- or two-sided
Only common tests should be described solely by name; describe more complex techniques in the Methods section.
- A description of all covariates tested
- A description of any assumptions or corrections, such as tests of normality and adjustment for multiple comparisons
- A full description of the statistical parameters including central tendency (e.g. means) or other basic estimates (e.g. regression coefficient) AND variation (e.g. standard deviation) or associated estimates of uncertainty (e.g. confidence intervals)
- For null hypothesis testing, the test statistic (e.g. F , t , r) with confidence intervals, effect sizes, degrees of freedom and P value noted
Give P values as exact values whenever suitable.
- For Bayesian analysis, information on the choice of priors and Markov chain Monte Carlo settings
- For hierarchical and complex designs, identification of the appropriate level for tests and full reporting of outcomes
- Estimates of effect sizes (e.g. Cohen's d , Pearson's r), indicating how they were calculated

Our web collection on [statistics for biologists](#) contains articles on many of the points above.

Software and code

Policy information about [availability of computer code](#)

Data collection No software was used for data collection.

Data analysis The custom Perl and Shell scripts for the computational pipeline of Cas13d-mediated circRNA screen (CDCscreen) to identify negatively selected functional circular RNAs in this paper is available at <https://github.com/YangLab/CDCscreen>. P value of negatively selected circRNA was computed by the permutation test of MAGeCK (v0.5.9.2). Raw pair-end gRNA library sequencing datasets were removed by cutadapt (v1.16), and aligned to gRNA library sequences with Bowtie (v1.1.2). RNA-seq reads quality were evaluated by FastQC (v0.11.5). Deep sequencing datasets were mapped with TopHat (TopHat v2.0.12, parameters: --microexon-search -g 1 -a 6 -m 2) and aligned to GRCh37/hg19 human reference genome with the UCSC Genes annotation (Human: hg19 knownGene.txt updated at 2013/06/30). Gene expression of linear mRNAs was determined by FPKM (Human hg19 refFlat.txt updated at 2017/04/09). CIRCExplore2 was used to identify circRNAs in multiple cell lines. Expression of circRNAs was determined by FPBCirc (Ma et al., Genomics Proteomics Bioinformatics, 2019). Sequences of back-spliced exons were extracted and used LiftOver tool (<http://genome.ucsc.edu/cgi-bin/hgLiftOver>) to identify orthologous coordinates between human and mouse. GO analysis was manually clustered with GeneCards (<https://www.genecards.org/>) and PubMed (<https://www.ncbi.nlm.nih.gov/pubmed/>). Functions of DEGs were manually checked by AmiGO 2 (<http://amigo.geneontology.org/amigo>). Statistical analyses was performed by R platform (R v3.5.1). Plots were generated with R platform (R v3.5.1) by using ggplot2 (v3.3.0), ggrepel (v0.8.1), corrplot (v0.84), pheatmap (v1.0.12), RColorBrewer (v1.1-2), ggpunr (v0.4.0), magrittr (v1.5) and ggbeeswarm (v0.6.0) packages. Histogram and line charts were plotted with GraphPad Prism 8 (v8.2.1). The protein levels were determined by WB and the intensity of the signals was quantified by ImageJ (v1.52).

For manuscripts utilizing custom algorithms or software that are central to the research but not yet described in published literature, software must be made available to editors and reviewers. We strongly encourage code deposition in a community repository (e.g. GitHub). See the Nature Research [guidelines for submitting code & software](#) for further information.

Data

Policy information about [availability of data](#)

All manuscripts must include a [data availability statement](#). This statement should provide the following information, where applicable:

- Accession codes, unique identifiers, or web links for publicly available datasets
- A list of figures that have associated raw data
- A description of any restrictions on data availability

All sequencing datasets have been deposited in the NCBI GEO (GSE149690, GSE149691, and GSE149692) and National Omics Data Encyclopedia (OEP000887, OEP000888 and OEP000889). The total RNA sequences of human H9, FB and PA1 cell lines were downloaded from NCBI GEO (GSE73325). RNA-seq datasets of SH-SY5Y were downloaded from NCBI GEO (GSE65926). RNA-seq datasets of HepG2, K562 cell lines and 11 different human tissues were downloaded from ENCODE Project Consortium (<https://www.encodeproject.org/>). AGO2 PAR-CLIP and miRNA-seq datasets of HEK293 cells were downloaded from NCBI GEO (GSE43573 and GSE58127). IGF2BP2 of eCLIP-seq datasets in K562 cells were downloaded from NCBI GEO (GSE91445). The Single-cell RNA-Seq transcriptome datasets in mouse preimplantation embryos were from NCBI GEO (GSE53386). All other data supporting the findings of this study are available from the corresponding author upon reasonable request.

Field-specific reporting

Please select the one below that is the best fit for your research. If you are not sure, read the appropriate sections before making your selection.

Life sciences Behavioural & social sciences Ecological, evolutionary & environmental sciences

For a reference copy of the document with all sections, see nature.com/documents/nr-reporting-summary-flat.pdf

Life sciences study design

All studies must disclose on these points even when the disclosure is negative.

| | |
|-----------------|--|
| Sample size | All knockdown experiments were performed with three independent replicates. All in vitro and in vivo screens were performed with two independent replicates. All other sample size numbers were listed in the corresponding figure legends. Sample sizes for these experiments were chosen based upon field standards and prior knowledge of experimental variation. |
| Data exclusions | No data were excluded. |
| Replication | The experimental findings in all figures were reproduced successfully. |
| Randomization | Samples were not randomized. Our experimental work-flow did not allow/need randomization. |
| Blinding | Blinding is not relevant to our study because it is not a subjective trial and the results presented here are purely based on objective description of our novel experimental technology. |

Behavioural & social sciences study design

All studies must disclose on these points even when the disclosure is negative.

| | |
|-------------------|---|
| Study description | Briefly describe the study type including whether data are quantitative, qualitative, or mixed-methods (e.g. qualitative cross-sectional, quantitative experimental, mixed-methods case study). |
| Research sample | State the research sample (e.g. Harvard university undergraduates, villagers in rural India) and provide relevant demographic information (e.g. age, sex) and indicate whether the sample is representative. Provide a rationale for the study sample chosen. For studies involving existing datasets, please describe the dataset and source. |
| Sampling strategy | Describe the sampling procedure (e.g. random, snowball, stratified, convenience). Describe the statistical methods that were used to predetermine sample size OR if no sample-size calculation was performed, describe how sample sizes were chosen and provide a rationale for why these sample sizes are sufficient. For qualitative data, please indicate whether data saturation was considered, and what criteria were used to decide that no further sampling was needed. |
| Data collection | Provide details about the data collection procedure, including the instruments or devices used to record the data (e.g. pen and paper, computer, eye tracker, video or audio equipment) whether anyone was present besides the participant(s) and the researcher, and whether the researcher was blind to experimental condition and/or the study hypothesis during data collection. |
| Timing | Indicate the start and stop dates of data collection. If there is a gap between collection periods, state the dates for each sample cohort. |
| Data exclusions | If no data were excluded from the analyses, state so OR if data were excluded, provide the exact number of exclusions and the rationale behind them, indicating whether exclusion criteria were pre-established. |

Non-participation

State how many participants dropped out/declined participation and the reason(s) given OR provide response rate OR state that no participants dropped out/declined participation.

Randomization

If participants were not allocated into experimental groups, state so OR describe how participants were allocated to groups, and if allocation was not random, describe how covariates were controlled.

Ecological, evolutionary & environmental sciences study design

All studies must disclose on these points even when the disclosure is negative.

Study description

Briefly describe the study. For quantitative data include treatment factors and interactions, design structure (e.g. factorial, nested, hierarchical), nature and number of experimental units and replicates.

Research sample

Describe the research sample (e.g. a group of tagged Passer domesticus, all Stenocereus thurberi within Organ Pipe Cactus National Monument), and provide a rationale for the sample choice. When relevant, describe the organism taxa, source, sex, age range and any manipulations. State what population the sample is meant to represent when applicable. For studies involving existing datasets, describe the data and its source.

Sampling strategy

Note the sampling procedure. Describe the statistical methods that were used to predetermine sample size OR if no sample-size calculation was performed, describe how sample sizes were chosen and provide a rationale for why these sample sizes are sufficient.

Data collection

Describe the data collection procedure, including who recorded the data and how.

Timing and spatial scale

Indicate the start and stop dates of data collection, noting the frequency and periodicity of sampling and providing a rationale for these choices. If there is a gap between collection periods, state the dates for each sample cohort. Specify the spatial scale from which the data are taken

Data exclusions

If no data were excluded from the analyses, state so OR if data were excluded, describe the exclusions and the rationale behind them, indicating whether exclusion criteria were pre-established.

Reproducibility

Describe the measures taken to verify the reproducibility of experimental findings. For each experiment, note whether any attempts to repeat the experiment failed OR state that all attempts to repeat the experiment were successful.

Randomization

Describe how samples/organisms/participants were allocated into groups. If allocation was not random, describe how covariates were controlled. If this is not relevant to your study, explain why.

Blinding

Describe the extent of blinding used during data acquisition and analysis. If blinding was not possible, describe why OR explain why blinding was not relevant to your study.

Did the study involve field work? Yes No

Field work, collection and transport

Field conditions

Describe the study conditions for field work, providing relevant parameters (e.g. temperature, rainfall).

Location

State the location of the sampling or experiment, providing relevant parameters (e.g. latitude and longitude, elevation, water depth).

Access & import/export

Describe the efforts you have made to access habitats and to collect and import/export your samples in a responsible manner and in compliance with local, national and international laws, noting any permits that were obtained (give the name of the issuing authority, the date of issue, and any identifying information).

Disturbance

Describe any disturbance caused by the study and how it was minimized.

Reporting for specific materials, systems and methods

We require information from authors about some types of materials, experimental systems and methods used in many studies. Here, indicate whether each material, system or method listed is relevant to your study. If you are not sure if a list item applies to your research, read the appropriate section before selecting a response.

Materials & experimental systems

| | |
|-------------------------------------|---|
| n/a | Involved in the study |
| <input type="checkbox"/> | <input checked="" type="checkbox"/> Antibodies |
| <input type="checkbox"/> | <input checked="" type="checkbox"/> Eukaryotic cell lines |
| <input checked="" type="checkbox"/> | <input type="checkbox"/> Palaeontology and archaeology |
| <input type="checkbox"/> | <input checked="" type="checkbox"/> Animals and other organisms |
| <input checked="" type="checkbox"/> | <input type="checkbox"/> Human research participants |
| <input checked="" type="checkbox"/> | <input type="checkbox"/> Clinical data |
| <input checked="" type="checkbox"/> | <input type="checkbox"/> Dual use research of concern |

Methods

| | |
|-------------------------------------|---|
| n/a | Involved in the study |
| <input checked="" type="checkbox"/> | <input type="checkbox"/> ChIP-seq |
| <input checked="" type="checkbox"/> | <input type="checkbox"/> Flow cytometry |
| <input checked="" type="checkbox"/> | <input type="checkbox"/> MRI-based neuroimaging |

Antibodies

Antibodies used

Anti-Flag antibody: Sigma, cat. no. F1804, clone M2.
 Anti-FAM120A antibody: Abcam, cat. no. ab156695.
 Anti-IGF2BP2 antibody: Abcam, cat. no. ab151463.
 Anti-RIG-I antibody: ABclonal, cat. no. A0550.
 Anti-AGO2 antibody: Sigma, cat. no. 03-110.
 Anti-ACTB antibody: Sigma, cat. no. A3854, clone AC-15.
 Anti-GAPDH antibody: GNI, cat. no. GNI4310-GH-S, clone 5A12.

Validation

All antibodies used in this study were validated by the vendor and are cited by multiple papers:
 Anti-Flag antibody: Sigma, cat. no. F1804. Validated in human cell lines for RIP and WB experiments in multiple publications: DOI: 10.1016/j.molcel.2017.05.023; DOI: 10.1016/j.cell.2019.03.046.
 Anti-FAM120A antibody: Abcam, cat. no. ab156695. Validated by company. "Reacting with mouse and human, and application for WB and IP." Refer to company website for detailed validation analysis and references.
 Anti-IGF2BP2 antibody: Abcam, cat. no. ab151463. Validated by company. "Reacting with human, and application for WB, IHC and IF." Refer to company website for detailed validation analysis and references.
 Anti-RIG-I antibody: ABclonal, cat. no. A0550. Validated in human cell lines for IP and WB experiments in the publication: DOI: 10.1016/j.cell.2019.03.046.
 Anti-AGO2 antibody: Sigma, cat. no. 03-110. Validated by company. "Reacting with human and bovine, and application for WB, IP and RIP." Refer to company website for detailed validation analysis and references.
 Anti-ACTB antibody: Sigma, cat. no. A3854. Validated in human cell lines for WB experiment in multiple publications: DOI: 10.1016/j.molcel.2017.05.023; DOI: 10.1016/j.cell.2019.03.046.
 Anti-GAPDH antibody: GNI, cat. no. GNI4310-GH-S. Validated in human cell lines for WB experiment in the publication: DOI: 10.1016/j.molcel.2017.05.023.

Eukaryotic cell lines

Policy information about [cell lines](#)

| | |
|--|--|
| Cell line source(s) | HT29, HeLa and 293FT cell lines were purchased from ATCC. |
| Authentication | These cell lines have been used in the lab for over 3 years. Authentications were not performed during this study. |
| Mycoplasma contamination | Cell lines have been tested negative for mycoplasma contamination by PCR methods. |
| Commonly misidentified lines (See ICLAC register) | No commonly misidentified cell line was used. |

Palaeontology and Archaeology

| | |
|---------------------|--|
| Specimen provenance | <i>Provide provenance information for specimens and describe permits that were obtained for the work (including the name of the issuing authority, the date of issue, and any identifying information).</i> |
| Specimen deposition | <i>Indicate where the specimens have been deposited to permit free access by other researchers.</i> |
| Dating methods | <i>If new dates are provided, describe how they were obtained (e.g. collection, storage, sample pretreatment and measurement), where they were obtained (i.e. lab name), the calibration program and the protocol for quality assurance OR state that no new dates are provided.</i> |

Tick this box to confirm that the raw and calibrated dates are available in the paper or in Supplementary Information.

| | |
|------------------|---|
| Ethics oversight | <i>Identify the organization(s) that approved or provided guidance on the study protocol, OR state that no ethical approval or guidance was required and explain why not.</i> |
|------------------|---|

Note that full information on the approval of the study protocol must also be provided in the manuscript.

Animals and other organisms

Policy information about [studies involving animals; ARRIVE guidelines](#) recommended for reporting animal research

| | |
|-------------------------|--|
| Laboratory animals | 4 to 5-week-old male BALB/c- <i>nu/nu</i> mice were used for subcutaneous xenograft tumor assays and in vivo screens. Around 8-week old B6D2F1 (C57BL/6 X DBA/2) female mice were superovulated and mated with the male B6D2F1 mice. 21-23 hr later, fertilized embryos were collected from oviducts. Mice were given free access to food and water, and were maintained under a 12/12 h light–dark cycle with controlled temperature (20-25°C) and humidity (50 ± 10%). |
| Wild animals | No wild animals were used in the study. |
| Field-collected samples | No field-collected samples were used in the study. |
| Ethics oversight | All animal procedures were performed under the ethical guidelines of the CAS Center for Excellence in Molecular Cell Science, Chinese Academy of Sciences (CAS). |

Note that full information on the approval of the study protocol must also be provided in the manuscript.

Human research participants

Policy information about [studies involving human research participants](#)

| | |
|----------------------------|---|
| Population characteristics | Describe the covariate-relevant population characteristics of the human research participants (e.g. age, gender, genotypic information, past and current diagnosis and treatment categories). If you filled out the behavioural & social sciences study design questions and have nothing to add here, write "See above." |
| Recruitment | Describe how participants were recruited. Outline any potential self-selection bias or other biases that may be present and how these are likely to impact results. |
| Ethics oversight | Identify the organization(s) that approved the study protocol. |

Note that full information on the approval of the study protocol must also be provided in the manuscript.

Clinical data

Policy information about [clinical studies](#)

All manuscripts should comply with the ICMJE [guidelines for publication of clinical research](#) and a completed [CONSORT checklist](#) must be included with all submissions.

| | |
|-----------------------------|---|
| Clinical trial registration | Provide the trial registration number from ClinicalTrials.gov or an equivalent agency. |
| Study protocol | Note where the full trial protocol can be accessed OR if not available, explain why. |
| Data collection | Describe the settings and locales of data collection, noting the time periods of recruitment and data collection. |
| Outcomes | Describe how you pre-defined primary and secondary outcome measures and how you assessed these measures. |

Dual use research of concern

Policy information about [dual use research of concern](#)

Hazards

Could the accidental, deliberate or reckless misuse of agents or technologies generated in the work, or the application of information presented in the manuscript, pose a threat to:

| | |
|--------------------------|---|
| No | Yes |
| <input type="checkbox"/> | <input type="checkbox"/> Public health |
| <input type="checkbox"/> | <input type="checkbox"/> National security |
| <input type="checkbox"/> | <input type="checkbox"/> Crops and/or livestock |
| <input type="checkbox"/> | <input type="checkbox"/> Ecosystems |
| <input type="checkbox"/> | <input type="checkbox"/> Any other significant area |

Experiments of concern

Does the work involve any of these experiments of concern:

No Yes

- Demonstrate how to render a vaccine ineffective
- Confer resistance to therapeutically useful antibiotics or antiviral agents
- Enhance the virulence of a pathogen or render a nonpathogen virulent
- Increase transmissibility of a pathogen
- Alter the host range of a pathogen
- Enable evasion of diagnostic/detection modalities
- Enable the weaponization of a biological agent or toxin
- Any other potentially harmful combination of experiments and agents

ChIP-seq

Data deposition

- Confirm that both raw and final processed data have been deposited in a public database such as [GEO](#).
- Confirm that you have deposited or provided access to graph files (e.g. BED files) for the called peaks.

Data access links

May remain private before publication.

For "Initial submission" or "Revised version" documents, provide reviewer access links. For your "Final submission" document, provide a link to the deposited data.

Files in database submission

Provide a list of all files available in the database submission.

Genome browser session (e.g. [UCSC](#))

Provide a link to an anonymized genome browser session for "Initial submission" and "Revised version" documents only, to enable peer review. Write "no longer applicable" for "Final submission" documents.

Methodology

Replicates

Describe the experimental replicates, specifying number, type and replicate agreement.

Sequencing depth

Describe the sequencing depth for each experiment, providing the total number of reads, uniquely mapped reads, length of reads and whether they were paired- or single-end.

Antibodies

Describe the antibodies used for the ChIP-seq experiments; as applicable, provide supplier name, catalog number, clone name, and lot number.

Peak calling parameters

Specify the command line program and parameters used for read mapping and peak calling, including the ChIP, control and index files used.

Data quality

Describe the methods used to ensure data quality in full detail, including how many peaks are at FDR 5% and above 5-fold enrichment.

Software

Describe the software used to collect and analyze the ChIP-seq data. For custom code that has been deposited into a community repository, provide accession details.

Flow Cytometry

Plots

Confirm that:

- The axis labels state the marker and fluorochrome used (e.g. CD4-FITC).
- The axis scales are clearly visible. Include numbers along axes only for bottom left plot of group (a 'group' is an analysis of identical markers).
- All plots are contour plots with outliers or pseudocolor plots.
- A numerical value for number of cells or percentage (with statistics) is provided.

Methodology

Sample preparation

Describe the sample preparation, detailing the biological source of the cells and any tissue processing steps used.

Instrument

Identify the instrument used for data collection, specifying make and model number.

| | |
|---------------------------|---|
| Software | <i>Describe the software used to collect and analyze the flow cytometry data. For custom code that has been deposited into a community repository, provide accession details.</i> |
| Cell population abundance | <i>Describe the abundance of the relevant cell populations within post-sort fractions, providing details on the purity of the samples and how it was determined.</i> |
| Gating strategy | <i>Describe the gating strategy used for all relevant experiments, specifying the preliminary FSC/SSC gates of the starting cell population, indicating where boundaries between "positive" and "negative" staining cell populations are defined.</i> |

Tick this box to confirm that a figure exemplifying the gating strategy is provided in the Supplementary Information.

Magnetic resonance imaging

Experimental design

| | |
|---------------------------------|---|
| Design type | <i>Indicate task or resting state; event-related or block design.</i> |
| Design specifications | <i>Specify the number of blocks, trials or experimental units per session and/or subject, and specify the length of each trial or block (if trials are blocked) and interval between trials.</i> |
| Behavioral performance measures | <i>State number and/or type of variables recorded (e.g. correct button press, response time) and what statistics were used to establish that the subjects were performing the task as expected (e.g. mean, range, and/or standard deviation across subjects).</i> |

Acquisition

| | |
|-------------------------------|---|
| Imaging type(s) | <i>Specify: functional, structural, diffusion, perfusion.</i> |
| Field strength | <i>Specify in Tesla</i> |
| Sequence & imaging parameters | <i>Specify the pulse sequence type (gradient echo, spin echo, etc.), imaging type (EPI, spiral, etc.), field of view, matrix size, slice thickness, orientation and TE/TR/flip angle.</i> |
| Area of acquisition | <i>State whether a whole brain scan was used OR define the area of acquisition, describing how the region was determined.</i> |
| Diffusion MRI | <input type="checkbox"/> Used <input type="checkbox"/> Not used |

Preprocessing

| | |
|----------------------------|--|
| Preprocessing software | <i>Provide detail on software version and revision number and on specific parameters (model/functions, brain extraction, segmentation, smoothing kernel size, etc.).</i> |
| Normalization | <i>If data were normalized/standardized, describe the approach(es): specify linear or non-linear and define image types used for transformation OR indicate that data were not normalized and explain rationale for lack of normalization.</i> |
| Normalization template | <i>Describe the template used for normalization/transformation, specifying subject space or group standardized space (e.g. original Talairach, MNI305, ICBM152) OR indicate that the data were not normalized.</i> |
| Noise and artifact removal | <i>Describe your procedure(s) for artifact and structured noise removal, specifying motion parameters, tissue signals and physiological signals (heart rate, respiration).</i> |
| Volume censoring | <i>Define your software and/or method and criteria for volume censoring, and state the extent of such censoring.</i> |

Statistical modeling & inference

| | |
|---|---|
| Model type and settings | <i>Specify type (mass univariate, multivariate, RSA, predictive, etc.) and describe essential details of the model at the first and second levels (e.g. fixed, random or mixed effects; drift or auto-correlation).</i> |
| Effect(s) tested | <i>Define precise effect in terms of the task or stimulus conditions instead of psychological concepts and indicate whether ANOVA or factorial designs were used.</i> |
| Specify type of analysis: | <input type="checkbox"/> Whole brain <input type="checkbox"/> ROI-based <input type="checkbox"/> Both |
| Statistic type for inference (See Eklund et al. 2016) | <i>Specify voxel-wise or cluster-wise and report all relevant parameters for cluster-wise methods.</i> |
| Correction | <i>Describe the type of correction and how it is obtained for multiple comparisons (e.g. FWE, FDR, permutation or Monte Carlo).</i> |

Models & analysis

n/a Involved in the study

Functional and/or effective connectivity

Graph analysis

Multivariate modeling or predictive analysis

Functional and/or effective connectivity

Report the measures of dependence used and the model details (e.g. Pearson correlation, partial correlation, mutual information).

Graph analysis

Report the dependent variable and connectivity measure, specifying weighted graph or binarized graph, subject- or group-level, and the global and/or node summaries used (e.g. clustering coefficient, efficiency, etc.).

Multivariate modeling and predictive analysis

Specify independent variables, features extraction and dimension reduction, model, training and evaluation metrics.